U.S. Department of
Transportation

**Federal Railroad
Administration**

Full-Scale Dynamic Testing of Locomotive Crashworthy Components

Office of Railroad Policy,
Development,
and Technology
Washington, DC 20590

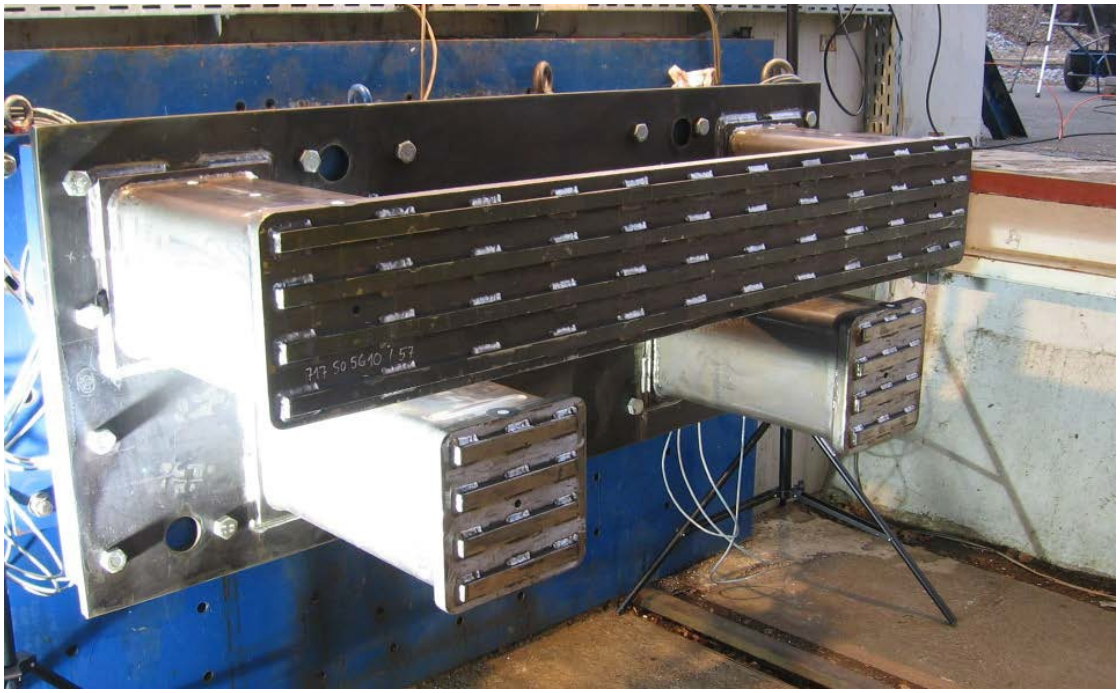

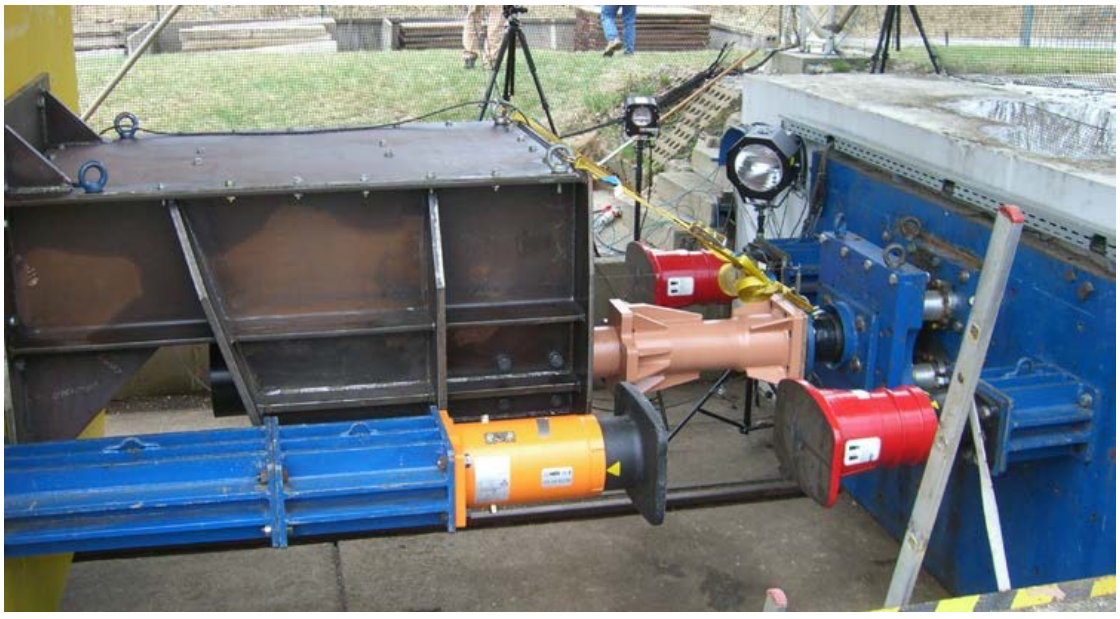

DOT/FRA/ORD-15/33

Final Report
October 2015

NOTICE

This document is disseminated under the sponsorship of the Department of Transportation in the interest of information exchange. The United States Government assumes no liability for its contents or use thereof. Any opinions, findings and conclusions, or recommendations expressed in this material do not necessarily reflect the views or policies of the United States Government, nor does mention of trade names, commercial products, or organizations imply endorsement by the United States Government. The United States Government assumes no liability for the content or use of the material contained in this document.

NOTICE

The United States Government does not endorse products or manufacturers. Trade or manufacturers' names appear herein solely because they are considered essential to the objective of this report.

REPORT DOCUMENTATION PAGE

Form Approved
OMB No. 0704-0188

1. AGENCY USE ONLY (Leave blank)	2. REPORT DATE	3. REPORT TYPE AND DATES COVERED
	October 2015	Technical Report – January 2014

4. TITLE AND SUBTITLE
Full-Scale Dynamic Testing of Locomotive Crashworthy Components

5. FUNDING NUMBERS

6. AUTHOR(S)
Patricia Llana and Dr. Richard Stringfellow

7. PERFORMING ORGANIZATION NAME(S) AND ADDRESS(ES)
TIAX, LLC
35 Hartwell Avenue
Lexington, MA 02421

8. PERFORMING ORGANIZATION REPORT NUMBER

9. SPONSORING/MONITORING AGENCY NAME(S) AND ADDRESS(ES)
U.S. Department of Transportation
Federal Railroad Administration
Office of Railroad Policy and Development
Office of Research, Development, and Technology
Washington, DC 20590

10. SPONSORING/MONITORING AGENCY REPORT NUMBER
DOT/FRA/ORD-15/33

11. SUPPLEMENTARY NOTES
COTR: Patricia Llana

12a. DISTRIBUTION/AVAILABILITY STATEMENT
This document is available to the public through the FRA Web site at http://www.fra.dot.gov.

12b. DISTRIBUTION CODE

13. ABSTRACT (Maximum 200 words)
The Office of Research, Development, and Technology of the Federal Railroad Administration (FRA) and the Volpe Center are evaluating new occupant protection technologies to increase the safety of passengers and operators in rail equipment. In view of the importance of override prevention in train-to-train collisions in which one of the vehicles is a locomotive, and the success of crash energy management technologies in cab-car-led passenger trains, the Volpe Center is evaluating the effectiveness of components that could be integrated into the end structure of a locomotive and are designed to mitigate the effects of a collision and, in particular, to prevent override of one lead vehicle onto the other. A research program has developed, fabricated, and tested two crashworthy components for the forward end of a locomotive: (1) a deformable anti-climber, and (2) a push-back coupler. Detailed designs were developed, and their performance was evaluated in large deformation dynamic finite element analysis (FEA). Designs were also developed for two test articles to verify the performance of the component designs in full-scale tests. The two test articles were fabricated and dynamically tested by means of rail car impact to verify their performance characteristics relative to specific requirements. The tests demonstrated the effectiveness of the two design concepts. Test results were consistent with finite element model predictions in terms of energy absorption capability, force-displacement behavior, and modes of deformation.

14. SUBJECT TERMS
locomotives, rail cars, override, collision, injury, impacts, testing, crash energy management, push-back coupler, anti-climber

15. NUMBER OF PAGES
81

16. PRICE CODE

17. SECURITY CLASSIFICATION OF REPORT	18. SECURITY CLASSIFICATION OF THIS PAGE	19. SECURITY CLASSIFICATION OF ABSTRACT	20. LIMITATION OF ABSTRACT
Unclassified	Unclassified	Unclassified	

NSN 7540-01-280-5500

Standard Form 298 (Rev. 2-89)
Prescribed by ANSI Std. 239-18
298-102

METRIC/ENGLISH CONVERSION FACTORS

ENGLISH TO METRIC	METRIC TO ENGLISH
LENGTH (APPROXIMATE)	**LENGTH (APPROXIMATE)**
1 inch (in) = 2.5 centimeters (cm)	1 millimeter (mm) = 0.04 inch (in)
1 foot (ft) = 30 centimeters (cm)	1 centimeter (cm) = 0.4 inch (in)
1 yard (yd) = 0.9 meter (m)	1 meter (m) = 3.3 feet (ft)
1 mile (mi) = 1.6 kilometers (km)	1 meter (m) = 1.1 yards (yd)
	1 kilometer (km) = 0.6 mile (mi)
AREA (APPROXIMATE)	**AREA (APPROXIMATE)**
1 square inch (sq in, in^2) = 6.5 square centimeters (cm^2)	1 square centimeter (cm^2) = 0.16 square inch (sq in, in^2)
1 square foot (sq ft, ft^2) = 0.09 square meter (m^2)	1 square meter (m^2) = 1.2 square yards (sq yd, yd^2)
1 square yard (sq yd, yd^2) = 0.8 square meter (m^2)	1 square kilometer (km^2) = 0.4 square mile (sq mi, mi^2)
1 square mile (sq mi, mi^2) = 2.6 square kilometers (km^2)	10,000 square meters (m^2) = 1 hectare (ha) = 2.5 acres
1 acre = 0.4 hectare (he) = 4,000 square meters (m^2)	
MASS - WEIGHT (APPROXIMATE)	**MASS - WEIGHT (APPROXIMATE)**
1 ounce (oz) = 28 grams (gm)	1 gram (gm) = 0.036 ounce (oz)
1 pound (lb) = 0.45 kilogram (kg)	1 kilogram (kg) = 2.2 pounds (lb)
1 short ton = 2,000 pounds (lb) = 0.9 tonne (t)	1 tonne (t) = 1,000 kilograms (kg)
	= 1.1 short tons
VOLUME (APPROXIMATE)	**VOLUME (APPROXIMATE)**
1 teaspoon (tsp) = 5 milliliters (ml)	1 milliliter (ml) = 0.03 fluid ounce (fl oz)
1 tablespoon (tbsp) = 15 milliliters (ml)	1 liter (l) = 2.1 pints (pt)
1 fluid ounce (fl oz) = 30 milliliters (ml)	1 liter (l) = 1.06 quarts (qt)
1 cup © = 0.24 liter (l)	1 liter (l) = 0.26 gallon (gal)
1 pint (pt) = 0.47 liter (l)	
1 quart (qt) = 0.96 liter (l)	
1 gallon (gal) = 3.8 liters (l)	
1 cubic foot (cu ft, ft^3) = 0.03 cubic meter (m^3)	1 cubic meter (m^3) = 36 cubic feet (cu ft, ft^3)
1 cubic yard (cu yd, yd^3) = 0.76 cubic meter (m^3)	1 cubic meter (m^3) = 1.3 cubic yards (cu yd, yd^3)
TEMPERATURE (EXACT)	**TEMPERATURE (EXACT)**
[(x-32)(5/9)] °F = y °C	[(9/5) y + 32] °C = x °F

QUICK INCH - CENTIMETER LENGTH CONVERSION

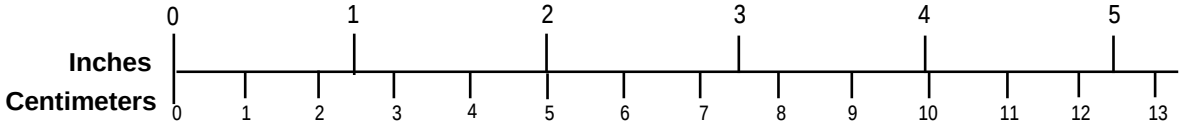

QUICK FAHRENHEIT - CELSIUS TEMPERATURE CONVERSIO

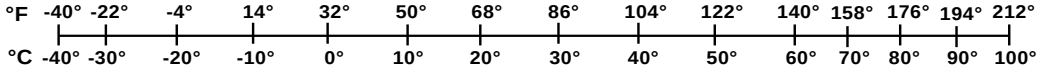

Contents

Figures

Tables

Executive Summary

In support of the Federal Railroad Administration (FRA) Passenger Equipment Safety Research Program, the Volpe Center has been conducting research to improve the structural crashworthiness of passenger rail cars and enhance occupant protection for crew and passengers. As a part of this work, crash energy management (CEM) strategies, in the form of crush zones incorporated at the ends of passenger cars, have been developed and tested with the goal of preserving occupant volume in passenger cars during accident scenarios.

In the event of a head-on collision between two trains, a considerable amount of energy must be dissipated. One of the potential consequences of such a collision is override, the lifting of one of the leading vehicles onto the other. Because of their great longitudinal strength and stiffness, locomotives are particularly susceptible to override when they collide with another vehicle, especially occupied passenger rail cars. The consequences of an override are often catastrophic. Research has shown, however, that the addition of a few structural features to the leading end of a locomotive can greatly reduce the propensity for override.

This program expands on concepts originally proposed in an earlier study of locomotive crashworthiness, by developing detailed designs for two crashworthy components (a push-back coupler and a deformable anti-climber) for a passenger trainlocomotive. The performance of these designs will be evaluated in dynamic impact tests of individual test articles and refined based on the results of the tests.

First, a set of requirements were defined to guide the development and evaluation of the designs. Most of the requirements were derived from existing American Public Transportation Association (APTA) [1] and Association of American Railroads (AAR) [2] standards. Draft designs were then developed for both components and integrated into the structure of a representative passenger locomotive, the MP40PH-3C “MPXpress” manufactured by MotivePower. Starting with a solid CAD structural model of the MP40, the forward end of the locomotive was modified, by integrating the two crashworthy components as well as structure to support the collision loads and distribute them into the existing car structure.

Because a crashworthy locomotive, when constructed, must necessarily be placed in service along with conventional equipment, the performance of the modified locomotive design was evaluated in three different collision scenarios:

- CEM locomotive to conventional locomotive
- CEM locomotive to cab car
- CEM locomotive to freight car.

In order to assess system performance in the three impact scenarios, four separate vehicle models were developed. The original and modified MP40 CAD models were used to construct finite element analysis (FEA) models of conventional and CEM locomotives. An FEA model of a state-of-the-art cab car developed in a prior program [3] was modified and used to represent the cab car. Finally, a model of a center-beam flat-car type freight car was constructed, using drawings supplied by the current manufacturer, TrinityRail. The individual vehicle models were then combined to form three distinct two-vehicle collision models.

In order to assess the robustness of the detailed designs that were developed, analyses for each of the three scenarios were conducted under ideal conditions (that is, with the vehicle couplers perfectly aligned) and also for two cases in which there would be a vertical offset of one vehicle with respect to another. In consultation with the Volpe Center, a 6-inch offset was chosen, evaluating both plus 6-inch and minus 6-inch cases. Based on the results of the analyses, some changes were made to the design of the crashworthy components. Designs for two separate test articles and fixtures were created for use in impact tests and were then evaluated using FEA-based simulations of the tests.

Because the test articles experience very high loads, the testing was performed by means of rail vehicle impact. For the deformable anti-climber device test, the test article was mounted to the crash wall. A flat, effectively rigid impactor was mounted onto the leading end of a rail car and run into the deformable anti-climber test article at an appropriate speed. However, for the push-back coupler test, the test article was mounted onto the leading end of a rail car and run into the crash wall at an appropriate speed. Motion and force data were collected using load cells, potentiometers, and other such instruments.

The impact tests were successful in demonstrating the effectiveness of the two concepts. Test results were consistent with model predictions both in terms of force-displacement behavior and modes of deformation.

The objective of the overall program was to develop and evaluate the effectiveness of designs for two components that could be integrated easily into the design of a passenger locomotive end structure: a deformable anti-climber and a push-back coupler. The program was divided into a Base effort and an Option A effort.

In the Base effort, detailed designs for the two components were developed, and the performance of each design was evaluated through large deformation dynamic FEA. Designs for two test articles that could be used to verify the performance of the component designs were also developed. A full FRA report on the research conducted for the Base effort, *Development, Fabrication, and Testing of Locomotive Crashworthy Components: Base Effort*, was produced [4].

This report summarizes the results of research performed for the Option A effort, which includes the testing conducted for the research program.

1. Introduction

FRA, with assistance from the Volpe Center, has been engaged for many years in active research aimed at improving the crashworthiness of rail vehicles. Much of this work has focused on mitigating the consequences of train-to-train collisions. This report summarizes the results of activities performed for Option A of the development, fabrication and testing of locomotive crashworthy components. Option A includes the fabrication and testing of the test articles designed in the Base effort.

1.1 Background

In the event of a head-on collision between two trains, a considerable amount of energy must be dissipated. One of the potential consequences of such a collision is override of one of the leading vehicles onto the other. Because of their high longitudinal strength and stiffness, locomotives are particularly susceptible to override when they collide with another vehicle. The consequences of an override are often catastrophic.

Accident investigations and other forms of research have shown that anti-climbing systems built into the ends of conventional locomotives are generally ineffective in preventing override. Impact between colliding couplers can induce dynamic vertical forces that cause one of the colliding vehicles to pitch significantly.

Research has further shown that conventional anti-climbing structures can deform on impact and form a ramp, increasing the likelihood of override [5]. As they crush longitudinally, conventional anti-climbers lose their vertical load-carrying capacity because of the substantial fracture that occurs as the anti-climber crushes. The longitudinal crush of the anti-climber causes fracture in the webs behind the face of the anti-climber. These fractured webs can still resist a longitudinal compression load, but they can no longer transmit a vertical shear load. This loss of vertical load-carrying capacity in conventional anti-climbers often leads to ramp formation, which promotes override. Such behavior was exhibited in a 23-mph rear end collision that occurred in Red Oak, Iowa, on April 17, 2011 [6]. As a result of the accident, several maintenance-of-way equipment cars overrode the impacting locomotive. The impacting locomotive's modular crew cab was detached and partially crushed as a result of being overridden (Figure 1), resulting in two fatalities. In order to be effective, an anti-climber must engage the end structures of opposing equipment and provide sufficient vertical load capacity to prevent such override.

Research has also shown that the propensity for override can be greatly reduced by the addition of a few structural features to the leading end of a locomotive [7], including the following:

- Push-back or breakaway couplers that allow the ends of the vehicles to interact prior to the buildup of large forces and moments that might lead to significant pitching of the vehicles with respect to one another
- Interlocking features and vertical strength characteristics that resist relative vertical motion of one vehicle with respect to the other so as to prevent the formation of a ramp
- Crushable zones that absorb collision energy so as to prevent uncontrolled deformation of interlocking features that might cause the formation of a ramp.

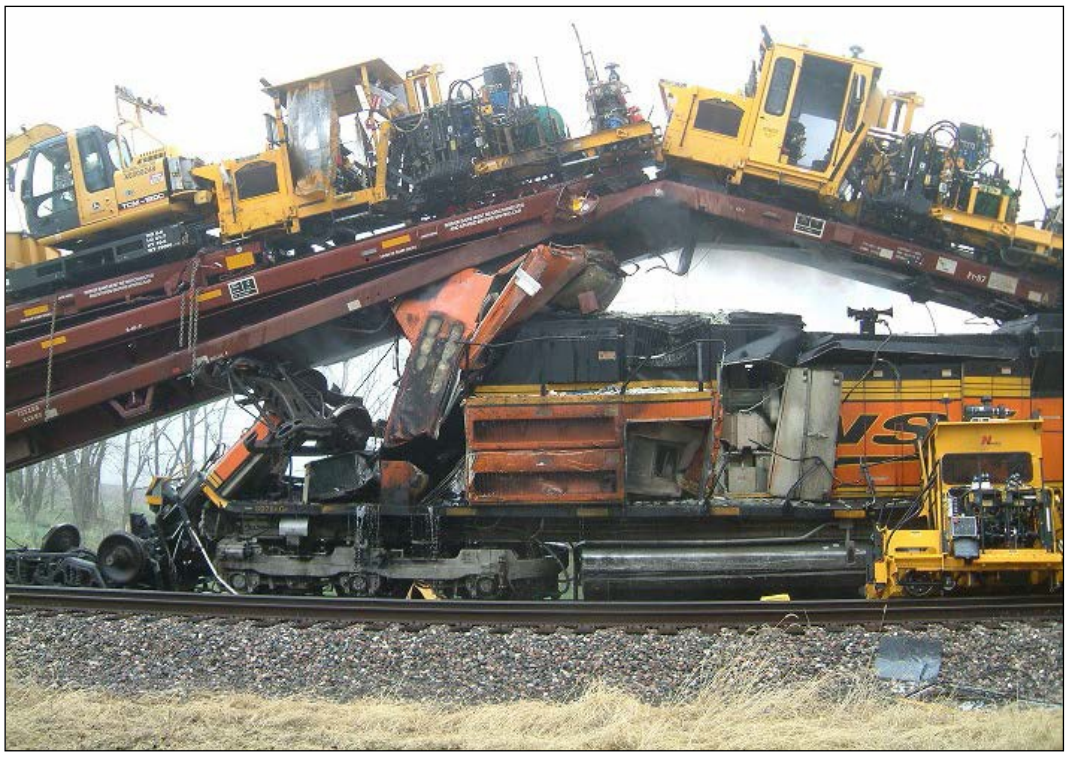

Figure 1. April 17, 2011, Collision: Red Oak, Iowa

Structural features such as those that are specifically put in place to mitigate the effects of a collision are common in rail vehicles designed according to the principles of CEM, which is a design strategy aimed at increasing occupant survivability during a collision, based on the notion that the energy of a collision can be dissipated in a controlled manner through strategic design and use of crush zones and other structural features.

CEM systems for passenger trains have been widely employed in Europe. In the United States, CEM systems are just now being developed. Beginning in 2000, FRA and the Volpe Center initiated a series of research programs aimed at developing a CEM system for a passenger train meant for use on the U.S. general railroad system. Those activities culminated in a full-scale collision test between a cab-car-led passenger train outfitted with a CEM system, traveling at 34 mph, and a standing, conventional locomotive-led train. This test, conducted in March 2006, clearly demonstrated the benefits of CEM design. Not only did the CEM train dissipate the energy of the collision through controlled deformation of crush zones throughout the length of the train, but the passenger train and the locomotive-led train both stayed on the track−in stark contrast to the results of a similar test of conventional equipment, in which the cab car overrode the locomotive (Figure 2).

Figure 2. Comparison of Outcomes of Full-Scale Train-to-Train Collision Tests
(a) Conventional passenger train. (b) CEM-based passenger train.

The successful outcome of the CEM train-to-train collision test helped to convince passenger rail operators that lives could be saved by employing crashworthiness features in their trains. The Southern California Regional Rail Authority (SCRRA) is in the process of incorporating a number of CEM-equipped cars into its Metrolink fleet. The Amtrak Cities Sprinter (ACS-64) locomotive, which was designed by Siemens Mobility for Amtrak and employs crashworthiness features, entered service in February 2014. Other examples of rail equipment with crashworthiness features include the Denton County Transportation Authority (DCTA) GTW articulated rail car designed by Stadler Rail, and the F125 locomotive designed by EMD for Metrolink. The Passenger Rail Investment and Improvement Act of 2008 (PRIIA) directed Amtrak to establish the Next Generation Corridor Equipment Pool Committee (NGEC) "to design, develop specifications for, and procure standardized next-generation corridor equipment." PRIIA requires that equipment purchased with Federal funds comply with specifications developed by the Section 305 NGEC, which require CEM.

1.2 Objectives

With the success of the passenger train CEM system, FRA and the Volpe Center are turning their attention back to locomotives. In the early stages of the locomotive research program [8] Arthur D. Little (now TIAX) examined the feasibility of incorporating anti-climbing systems in cab cars and locomotives. In the more recent stages of the program, TIAX led the effort to develop and evaluate design concepts for improved locomotive override protection. Concepts for crashworthy components that were identified include: push-back couplers, deformable anti- climbers, and crush zones built into the forward end of the locomotive underframe.

The objective of the overall program is to develop, and evaluate the effectiveness of, designs for two components that could be integrated easily into the design of a passenger locomotive end structure: a deformable anti-climber and a push-back coupler. The program includes a Base effort and an Option A effort.

1.3 Overall Approach

In the Base program, a set of requirements was defined that would guide the development and evaluation of the designs. The design requirements include performance requirements, geometric requirements, operational requirements, and fabrication requirements. The energy absorption requirements and many of the other crashworthiness specifications are derived from experience gained in other crashworthiness programs. Most of the strength requirements and some of the crashworthiness specifications are derived from APTA [9, 10] and AAR [11] standards. All the requirements are consistent with CFR 49 Part 229 [12], APTA SS-C&S-034- 99 Rev 2 [13], and APTA PR-RP-C&S-019-11 [14]. During the development process, the design requirements evolved as the designs were evaluated. In the interest of efficiency, the final design requirements are described in the Base effort report [15].

Draft designs were developed for the components and integrated into the structure of a representative passenger locomotive, the MP40PH-3C "MPXpress" manufactured by MotivePower. Starting with a solid CAD structural model of the MP40, the forward end of the locomotive was modified, integrating the two crashworthy components as well as structural elements to support the collision loads and distribute them into the existing car frame.

A crashworthy locomotive, when constructed, must be placed in service along with conventional equipment. For this reason, the performance of the modified locomotive design was evaluated in three different collision scenarios:

- CEM locomotive to conventional locomotive
- CEM locomotive to cab car
- CEM locomotive to freight car.

In order to assess system performance in each of the three scenarios, four separate vehicle models were developed: (1) conventional locomotive, (2) CEM locomotive, (3) cab car, and (4) freight car. The original and modified MP40 CAD models were used to construct FEA models of conventional and CEM locomotives. An FEA model of a state-of-the-art cab car developed in a prior program [16] was modified and used to represent the cab car. Finally, a model of a center-beam, flat-car type of freight car was constructed, using drawings supplied by the current manufacturer, TrinityRail. The individual vehicle models were then combined to form three distinct two-vehicle collision models.

Analyses were conducted for each of the three scenarios. Based on the results of the analyses, some changes were made to the design of the crashworthy components. Designs were created for two separate test articles and fixtures for use in impact tests, then evaluated using FE-based simulations of the tests. This marked the end of the Base program, the results of which are detailed in the Base effort report [17]. Drawings of the MP40 retrofit designs for both components are available on the FRA website [18].

In the Option A program, the two test articles designed in the Base program were fabricated and tested by means of a dynamic impact test in order to verify certain performance characteristics of the two components relative to requirements. The test articles were fabricated by BEPeterson in Avon, MA. The fabricated test articles were then shipped to Görlitz Germany, where they were tested by TÜV SÜD in April 2012, under the direction of TIAX and its subcontractor, Simpson Gumpertz and Heger (SGH).

1.4 Scope

Initially, the scope of the Option A program included the fabrication, shipment, and testing of the two crashworthy components. An additional task was added to the Option A program for the purpose of fabricating and quasi-statically crush-testing subcomponent test articles for the deformable anti-climber. The subcomponent test articles were also fabricated by BEPeterson and quasi-statically tested at SGH facilities in Waltham, MA. As part of this added task, tensile tests were conducted at SGH in order to generate complete true stress-true strain curves for the A572-50 steel that was used to construct the key elements of the deformable anti-climber.

1.5 Organization of the Report

A description of the test articles is provided in Section 2. Preliminary testing is described in Section 3, which includes material testing and subcomponent testing of the crush tubes. Section 4 details the fabrication and quality control of the test articles. The activities involved in conducting the component tests, including pre-test calculations, are provided in Section 5. In Section 6, a comparison is made between the test results and the pre-test predictions. The report ends with a summary and conclusions in Section 7.

2. Description of Test Articles

The locomotive platform chosen for development was a MotivePower MPXpress MP40PH-3C. The two test articles are described briefly in the sections below. More detailed descriptions of the test articles and the designs of the respective locomotive components they represent are included in the final report to the Base program [19].

2.1 Push-back Coupler

The push-back coupler test article is pictured in Figure 3. It comprises a support assembly that features two I-beams welded to a large back plate and reinforced with triangular gussets. A top plate is bolted across the top flanges of the I-beams, and a bottom plate is welded between the bottom flanges. Side plates are welded to the bottoms of the I-beams and reinforced with horizontal stiffener plates. A front plate and two sets of gussets—one vertical and one angled back—provide further stiffness to the support assembly.

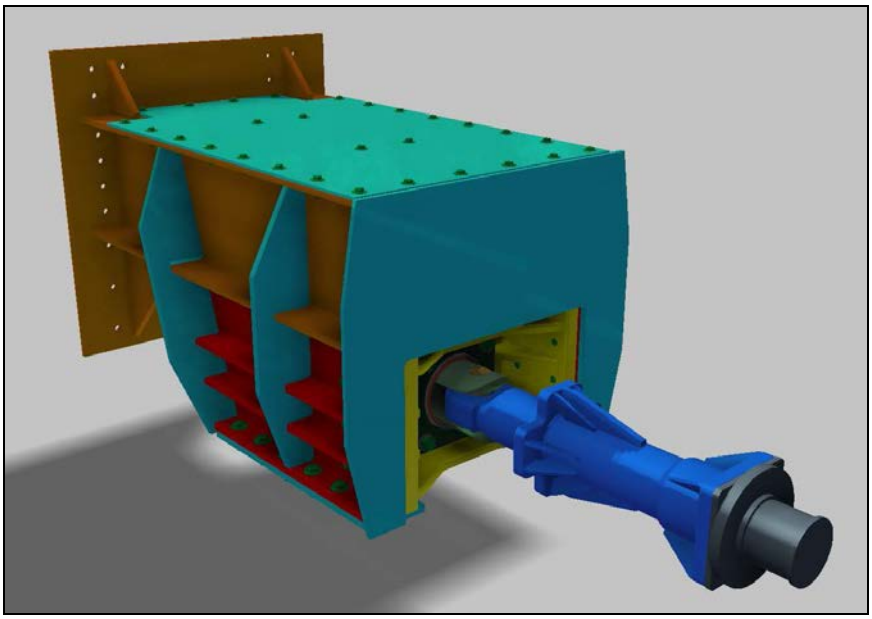

Figure 3. The Push-Back Coupler Test Article

The push-back coupler test article features a push-back coupler designed and manufactured by Voith Turbo. Elastomeric elements provide reversible energy absorption for low-speed impacts. A deformation tube provides irreversible energy absorption for higher-speed impacts. On compression, an element attached to the inboard end of the coupler moves against the elastomeric elements. With enough stroke and load, this piece eventually causes the deformation tube to activate. The moving piece has an outer diameter that is larger than the inner diameter of the deformation tube. The push-back force is a function of the interference between the inner and outer tubes. The stroke over which energy is absorbed depends on the tube length.

The force-displacement characteristics of the push-back coupler used in this program are as follows: the load builds up nearly linearly from zero to 3,000 kN (674,400 lbf) over about 3

inches as a rubber spring compresses. With additional stroke, the deformation tube activates and the load stays effectively constant at 674,000 lbf throughout the stroke of the deformation tube.

The push-back coupler is mounted to a sliding lug assembly (indicated in yellow in Figure 3), which in turn is bolted to the side plates by 12 specially designed shear bolts. A coupler extension (shown in blue) is connected to the coupler with a standard coupler pin arrangement. A feature has been added to the coupler extension so that, when the total stroke of the coupler reaches 18" (457 mm), the back surface of the feature will impact the front surface of the sliding lug mounting block, thereby causing the load to spike and shear the bolts, securing the sliding lug within the side plates. Once the bolts have broken, there is no further mechanism of energy absorption, and the force drops to zero.

The shear bolts are designed to break at a design load of 12 bolts × 88 kips = 1,056 kips (4,700 kN). A drawing detail that shows the shear bolt connection arrangement is pictured in Figure 4(a). A shear bolt is pictured in Figure 4(b) together with its two bushings. Shear bolts are tightened to a torque of 735 N-m. The front of the extension is bolted to a "tup"—a 6-inch round cylindrical impactor that is slightly rounded at its forward end and includes a 5,000 kN (1,125 kips) load cell. The tup is not part of the production design and is present for testing only.

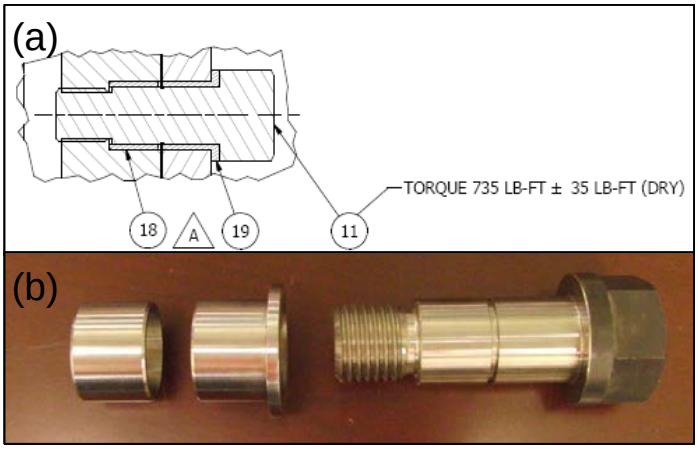

Figure 4. Shear Bolt Connection Arrangement
(a) Drawing detail shows the shear bolts installed through the walls of the side plate assembly and the sliding lug assembly. (b) Photograph of a shear bolt and its two bushings. (Shear bolts were designed and manufactured by Voith Turbo.)

The sequence of operation of the push-back coupler operation is as follows:

1. The draft gear is compressed by about 3 inches (75 mm).
2. The push-back coupler energy absorber begins its stroke at a load of about 675 kips (3,000 kN).
3. Energy is absorbed for a stroke of 15 inches (380 mm), bringing the total stroke to 18 inches (457 mm).
4. The special feature of the coupler extension contacts and loads the coupler mounting flange.
5. Load builds up rapidly in the shear bolts, to a value of about 1,056 kips (4,900 kN).
6. The shear bolts fail essentially simultaneously.
7. The sliding lug pushes back into the main housing without load.

The design force versus displacement curve for the push-back coupler test article is shown in Figure 5.

Figure 5. Design Force-Displacement Curve for the Push-Back Coupler Test Article

The push-back coupler test article weighs about 6,600 lb. A breakdown in weight for the test article is shown in Table 1.

Table 1. Weight Breakdown for the Push-Back Coupler Test Article

Item	Quantity	Weight	Total Weight
Support Beam Assembly	**1**	**2,309.7**	**2,309.7**
Base Plate	1	646.7	**646.7**
Top Beam	2	501.1	**1,002.2**
Top Gusset	2	10.5	**21.0**
Bottom Gusset	2	51.0	**102.0**
Bottom Plate	1	387.6	**387.6**
Top Angle	1	21.2	**21.2**
Stiffener Plate	2	64.5	**129.0**
Sliding Lug Assembly	**1**	**1,039.2**	**1,039.2**
Front Plate	1	473.6	**473.6**
Side Plate	2	202.0	**404.0**
Middle Gusset	4	9.9	**39.6**
Top/Bottom Gusset	2	61.0	**122.0**
Side Wall Assembly	**2**	**414.7**	**829.4**
Side Wall	1	246.6	**246.6**
Stopper Plate	1	20.7	**20.7**
Top Stiffener Plate	1	54.2	**54.2**
Middle Stiffener Plate	1	49.9	**49.9**
Bottom Stiffener Plate	1	43.3	**43.3**
Middle Plate	**2**	**65.9**	**131.8**
Front Plate	**1**	**225.7**	**225.7**
Back Plate	**2**	**107.9**	**215.8**
Top Plate	**1**	**289.1**	**289.1**
Rail Stopper Plate	**2**	**85.3**	**170.6**
Shear Bolts with Bushings	**12**	**1.9**	**22.8**
Push-Back Coupler	**1**	**793.8**	**793.8**
Push-Back Coupler Extension	**1**	**573.3**	**573.3**
		Grand total:	**6,601.2**

2.2 Deformable Anti-climber

The deformable anti-climber test article (Figure 6), consists of four crush tubes mounted on a large, thick back plate that is designed, in turn, to be mounted directly to an instrumented test wall. The two upper crush tubes are positioned 12.5 inches above the lower crush tubes. They are connected by a 68-inch wide × 11-inch high × 1.0-inch thick front plate that has four 0.5-inch thick × 1.0-inch high × 66-inch long bars, centered vertically 2.5 inches apart from one another, welded to its front surface. The two lower crush tubes are 2 inches longer than the two upper crush tubes, spaced closer together laterally (38.5 inches center-to- center vs. 57 inches center-to-center for the upper tubes). Each tube has its own 11-inch square × 1.0-inch thick front plate, with a similar set of four bars welded to it, each 0.5 inch thick × 1.0 inch high × 9 inches long, spaced at 2.5-inch intervals.

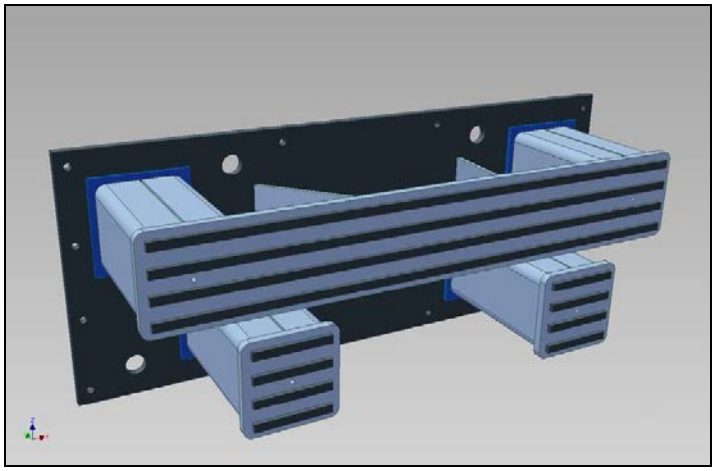

Figure 6. The Deformable Anti-climber Test Article

Each of the tubes has a ¼-inch wall thickness. In addition, each tube has four rounded, 0.125-inch deep slots cut into it to promote controlled folding: two on the inside and two on the outside (Figure 7). The two inside slots are cut into the sides of the tubes, and the two outside slots are cut into the top and bottom of the tubes, across the welded seam that joins the two halves of each tube. The slots are centered about 2.375 inches from the front of each tube.

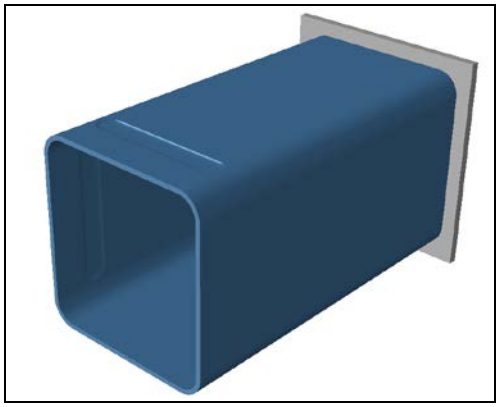

Figure 7. Crush Tube (Revised Design) with Front Plate Removed

In addition to the four crush tubes, there are two 0.5-inch thick angled support plates that provide stability and vertical strength to the upper set of crush tubes. They are oriented vertically and positioned approximately 17 inches apart where they are welded to the front plate and 28.75 inches apart where they are welded to the back plate.

The deformable anti-climber test article weighs about 1,275 lb. A breakdown for the weight of the test article is shown in Table 2.

Table 2. Weight Breakdown for the Deformable Anti-climber Test Article

Item	Quantity	Weight	Total Weight
Top Crush Tube Assembly	**1**	**373.3**	**373.3**
Crush Tube	2	43.6	**87.2**
Front Plate	1	211.5	**211.5**
Front Plate Bar	4	9.3	**37.2**
Back Plate	2	18.7	**37.4**
Lower Crush Tube Assembly	**2**	**106.7**	**213.4**
Crush Tube	1	48.8	**48.8**
Front Plate	1	34.0	**34.0**
Front Plate Bar	4	1.3	**5.2**
Back Plate	1	18.7	**18.7**
Angled Support Plate	**2**	**22.7**	**45.4**
Large Back Mounting Plate	**1**	**642.3**	**642.3**
		Grand total:	**1,274.4**

3. Preliminary Testing

Given uncertainties about the crush performance of the crush tube components of the deformable anti-climber due to the uniqueness of the slotted-tube design, quasi-static tests on individual crush tubes were conducted to evaluate their performance and provide an opportunity to modify the design of the tubes prior to the dynamic test.

Two crush tube assemblies fabricated for this purpose were quasi-statically tested in August 2011 at the facilities of SGH in Waltham, MA. The results of these two tests indicated that certain features of the tube design needed to be improved. A third crush tube assembly was fabricated for this purpose. In addition, one of the two original tube assemblies, which had been crushed only partially, was repaired, with the crushed end cut off to make a shorter tube.

In addition to crush-testing, a series of tensile tests were conducted to determine the stress-strain behavior, through fracture, of the specific lot of A572-50 steel that would later be used to fabricate both the subcomponent test articles and the crush tube components of the deformable anti-climber test article. The results of these tests are presented first.

3.1 Materials Tests

A one-foot by one-foot sample of the 0.25-inch thick A572-50 material was provided to SGH by BEPeterson (the fabricator of the test articles, as described in Section 4 below). SGH conducted the tests using the following procedure:

1. Six round bar-type tensile specimens were fabricated from the A572-50 material supplied. Each specimen featured a gage length of 0.5 inches and a diameter in the gage region of approximately 0.16 inches, yielding a cross-sectional area of approximately 0.02 square inches.
2. An initial test was conducted to fracture. Strain was measured with an extensometer. The machine cross-head displacements at maximum load and at fracture were recorded.
3. A second test was conducted to a cross-head displacement approximately halfway between the two cross-head displacements measured in the first test.
4. Three additional tests were conducted with cross-head displacements in a range between those corresponding to maximum load and fracture.
5. The final diameters of the necked sections of each test specimen were measured and used to calculate a diametral strain.
6. A polynomial fit to the six measured stress/strain values was made to determine a complete stress-strain curve. The individual data points and polynomial fit are shown in Figure 8.

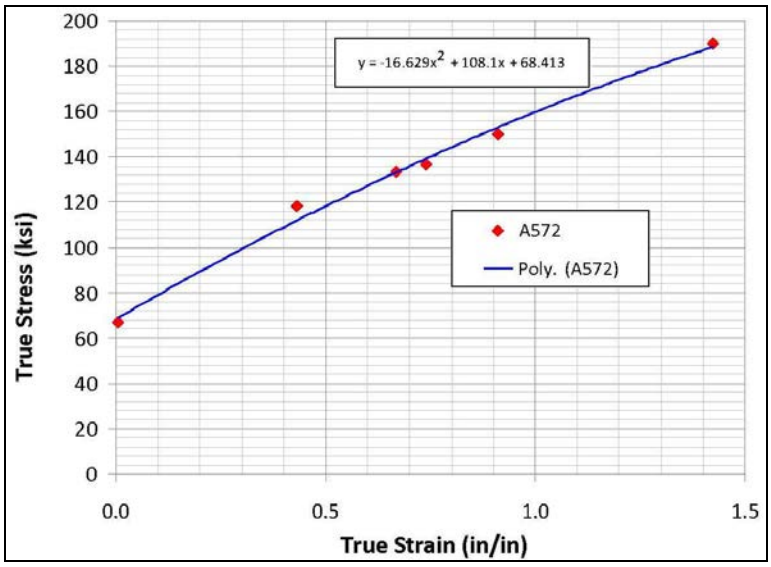

Figure 8. True Stress-Strain Curve for A572-50 Fit to Measured Data

These data indicate a fracture strain in uniaxial tension of 1.42. This value was used as the basis for selecting parameters of a Bao-Wierzbicki failure model that was implemented in FEA models of tube crush.

3.2 Subcomponent Crush Tests for Original Tube Design

3.2.1 Fabrication

Two identical subcomponent test articles were fabricated, based on a design derived from the lower crush tube assembly (drawing #TC09016-008), which is part of the main assembly (drawing #TC09016-0012) for the deformable anti-climber test article. The subcomponent test article designs are identical to the lower crush tube assembly, with one exception: they do not have the four short rectangular bars (drawing #TC09106-0017) welded to the front plate of the crush tube.

Each tube featured a 1-inch wide internal slot all around its inside surface, about 1 inch from the forward end of the tube. This slot was added to promote folding of the tube and reduce the initial impact load. TIAX's design subcontractor, Taylor Raynauld Amar & Associates (TRA), prepared and delivered to TIAX a drawing package for the subcomponent test article. (The "Crush Tube for Static Test Assembly" drawing was labeled as #TC09106-0055.) The slot design is illustrated in Figure 9, which shows the design of the slot cut into the front inside wall of the half-tube. Two half-tubes are welded together to form the crush tube.

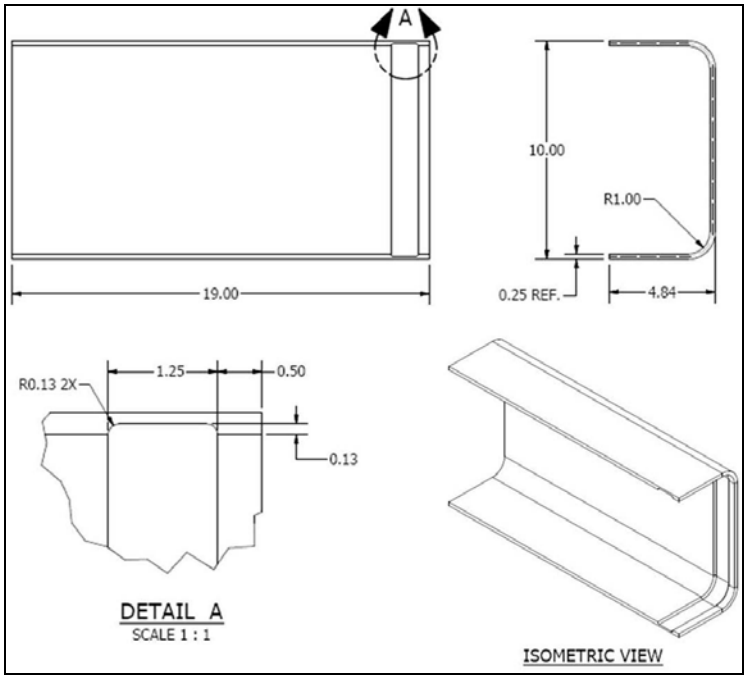

Figure 9. Design of Slot Cut into Front Inside Wall of Half-Tube
Excerpt from Drawing #TC09106-0055.

The two identical test articles were fabricated by BEPeterson in Avon, MA (see Section 4 below). A quality control review conducted by BEPeterson revealed that the final cross-sectional dimensions of the tubes after welding was 9.75 by 10 inches, rather than 10 by 10 inches, as specified. Given the desire to have all the material for the tubes come from the same lot of steel, and the expectation that the effect on the behavior of the tubes would be limited, this deviation from the dimensional requirements for the tubes was approved by TIAX and by the Volpe Center. The fabricated tubes were inspected by TIAX and found to be otherwise within dimensional tolerances.

3.2.2 Pre-test FEA

Prior to the crush testing of subcomponent test articles, an FEA-based simulation of the test was conducted, using the measured true stress-strain data to formulate a material model. Note that these calculations, as well as all others referred to in this report, were conducted using the ABAQUS finite element program, version 6.8-4. Two analyses were performed: one that did not include material failure, and one that included a material failure model based on the Bao-Wierzbicki criterion, using the estimated fracture strain of 1.42 determined in the tensile tests as the basis for the selection of model parameters. The FEA results indicated that no fracture occurred using these parameters in the failure model.

The FEA model is shown in Figure 10. Approximately 100,000 shell elements were used, with a characteristic element size of 0.1 inches, and one shell through the thickness. As with the test article FEA model, the geometry of the wall of the tube was offset outward by up to 0.125 inches in the slotted region. In addition, the thicknesses of the elements in this region were reduced accordingly.

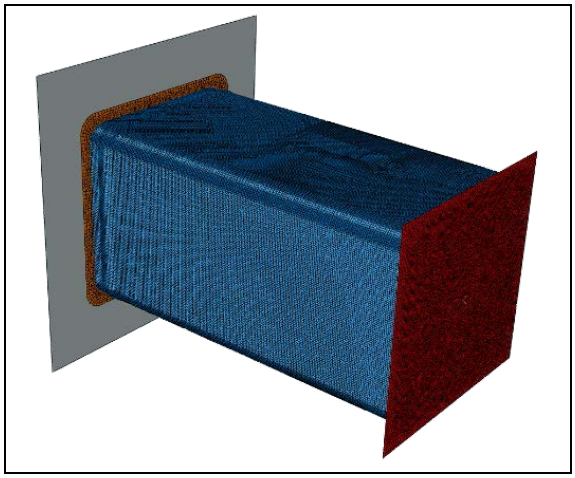

Figure 10. Pre-test FEA Model of Crush Tube (Original Design)

The predicted deformation modes for three levels of crush (with the end plate removed) are illustrated in Figure 11. The entire slotted region deforms first, as expected, mushrooming outward all around the tube. Contours of equivalent plastic strain indicate that large strains arise in the slotted region, particularly near the four rounded corners of the tube. Once this area has folded over onto itself, the remainder of the tube begins to deform, in a manner that is typical of square-tube folding and collapse. Localized regions of large plastic strain arise in the corners of the tube as it continues to crush.

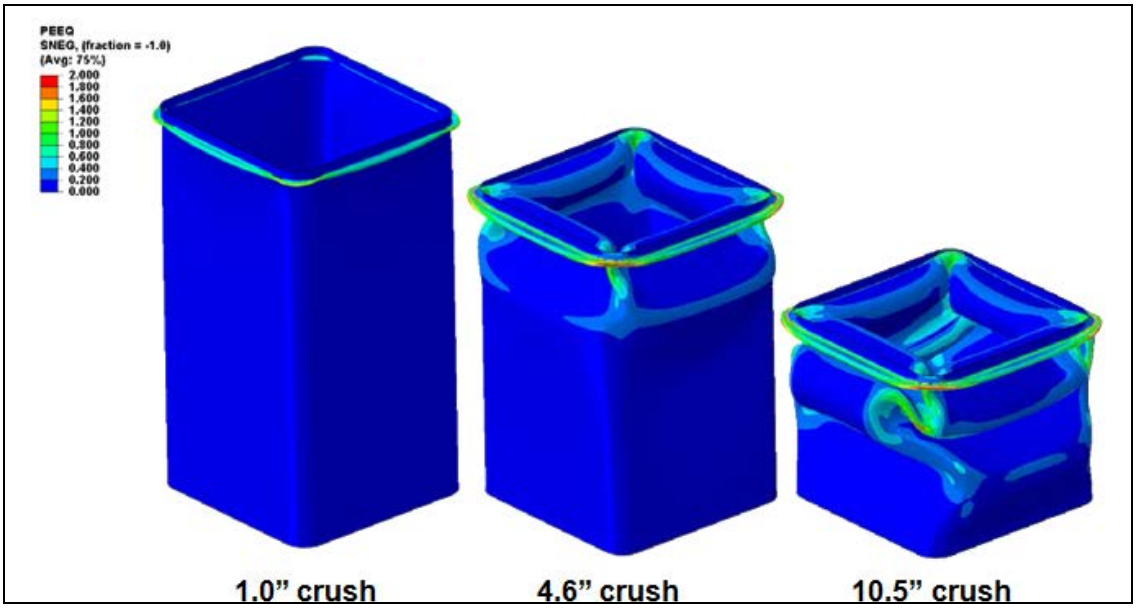

Figure 11. Pre-test FEA Model: Equivalent Plastic Strain at Several Levels of Displacement

The resulting force-displacement curve is shown in Figure 12. The force quickly builds to 210 kips. Then the slot folds, lowering the force to 130 kips. The slot then finishes folding, and the load builds up again. The load then reaches approximately 420 kips, whereupon a second fold begins to form. The force then drops to a range between 110 and 200 kips as the tube continues

to fold, until the folds begin to consolidate at around 14 inches of crush and the load rapidly builds up again. The predicted energy absorption after 14 inches of crush is 214 ft-kips.

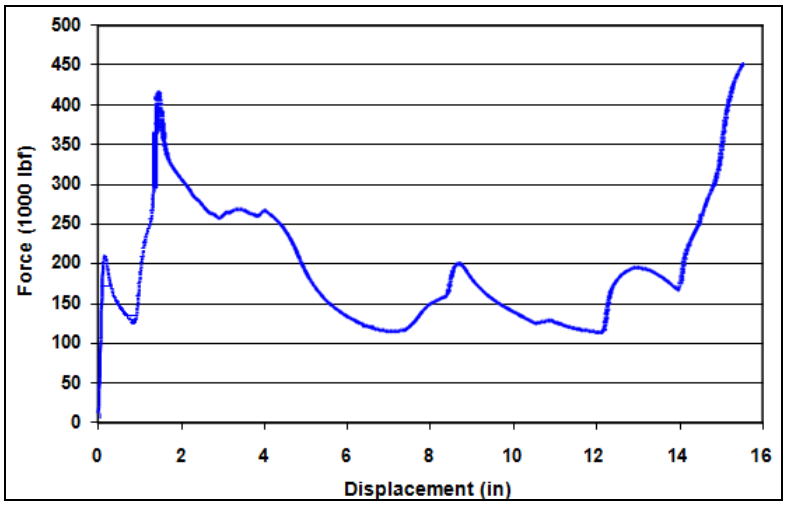

Figure 12. Pre-test FEA Model Predicted Force-Crush Curve

3.2.3 Test Plan

A test plan was prepared by SGH and reviewed by TIAX and by the Volpe Center. Key specifications of the plan included:

- Forney 600 kip-capacity electro-mechanical testing machine, with a stroke limit of over 25 inches
- Displacement rate of approximately 1.0 inches per minute
- Expected maximum crush of 11 to 14 inches before reaching the 600-kip load capacity of the machine and stopping the test
- Stroke measured with a string potentiometer (Micron Epsilon WPS 750 mm)
- Load measurement based on hydraulic pressure in the test machine
- Still images taken from a single camera before and after the test and during the test at 1-inch intervals of displacement
- A video of the test from a single camera
- Data acquisition from a National Instruments DAQ system at a sampling rate of 2 Hz.

3.2.4 Test Results

The test on the first crush tube was conducted at SGH in August 2011. In attendance were personnel from TIAX, the Volpe Center, and SGH.

The test was started at the prescribed load rate of 1.0 inches per minute. After approximately one inch of crush, loud popping noises were heard, signifying the initiation of fracture. Continued crush produced further audible signs of cracking. The specimen was unloaded after approximately 2.4 inches of crush, and examined, revealing the formation of vertical cracks

about 1.5 inches away from each of the corners of the tube (Figure 13). The test was continued, and as the tube deformed, two opposing sides of the plate (the "front" and "back" of the specimen) began to peel away from the tube due to continued propagation of the vertical cracks. The test was stopped after 15.5 inches of crush. When the tube was completely unloaded and removed from the testing machine, the entire top plate had separated from the rest of the tube due to the propagation of a crack all the way around the slotted region of the tube. A photograph of the tube after the test (minus the separated top end) is shown in Figure 14.

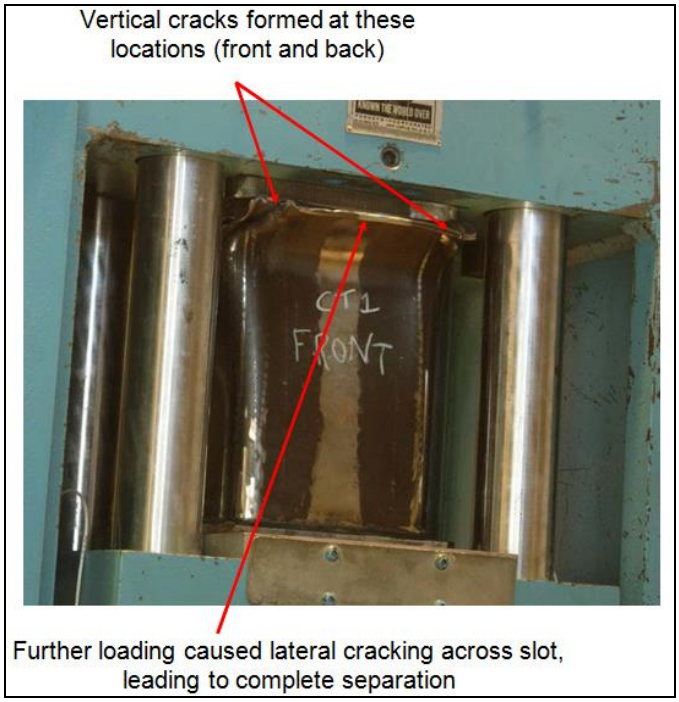

Figure 13. Photograph of the First Test Article
Displacement of approximately 2.4 inches, showing vertical cracks near the corners of the tubes in the slotted region and lateral cracks across the slot.

Figure 14. Post-test Photograph of First Test Article
Separated top end of test article not shown.

Because of the expectation of fracture, the test on the second crush tube was conducted at a slower rate (0.25 inches per minute), and the test was stopped much more often for inspection. This test was stopped completely after about 2 inches of displacement, following a loud pop indicating fracture. No fractures were clearly visible from the outside of the tube; however, a cut-out made after the test through the corner of the tube at the location of the slot revealed that a lateral crack had formed, likely in each of the four corners of the tube (Figure 15).

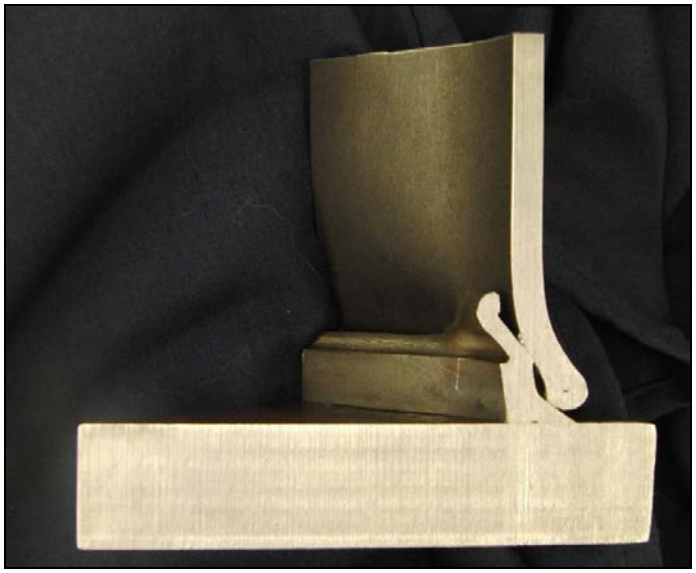

Figure 15. Cross-section Through Slot at Corner of Crush Tube Revealing Lateral Fracture

A comparison of the pre-test model prediction of force-displacement curve with test results is shown in Figure 16. The model seems to do a good job of predicting behavior early on for both tests. Once fracture initiates, the behavior in the test begins to diverge from model predictions, as one might expect. Nonetheless, the general characteristics of the curves (load magnitudes, size and shape of undulations) are similar. The measured crush energy after 14 inches of crush is 220 ft-kips for the first test, which is only about 3% more than the predicted value.

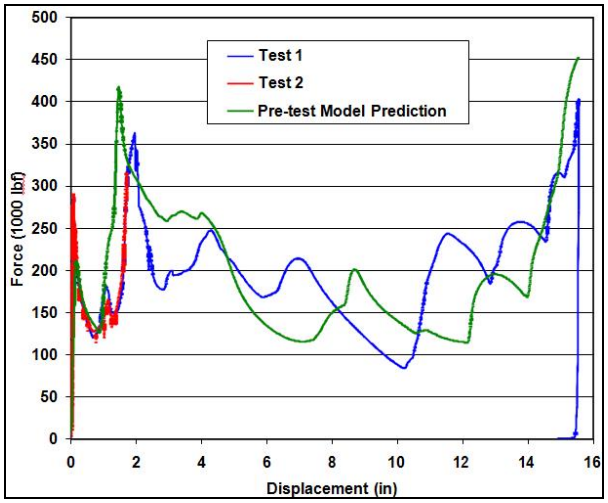

Figure 16. Comparison of Pre-test Predictions and Test Results for Force vs. Displacement

3.2.5 Post-test FEA

Clearly, the pre-test FEA did not predict the fracture that occurred during the test. To better account for the complex geometry of the slot, a solid element-based FEA model simulating the test was constructed (Figure 17). It features a 0.04-inch characteristic element length on the surface of the tube and has five elements through the thickness of the tube, including the slot regions. There are approximately 675,000 elements in total, taking advantage of the quarter-symmetry of the tube.

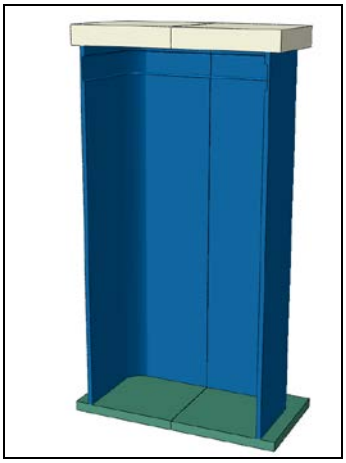

Figure 17. Revised, Solid Element-Based FEA Model

The revised model, using the same material failure law used in the shell-based model, indicated that some fracture would eventually be initiated, but not at the displacement levels at which it was initiated during the test, nor to the extent observed in the test. To capture the fracture initiation at approximately the same extent of displacement at which it was observed in the test, it was necessary to lower the fracture strain parameter by 50%, to 0.71. (Further investigation into why the fracture strain needed to be reduced so much relative to the measured value suggested that it was partly due to the manner in which the ABAQUS failure model treats the failure strain parameter, and could also be partly due to directional differences in ductility, the effect of residual stresses that arise in the corners of the tube during forming, and other difficulties in defining the failure strength of the material with limited test data.) When this change was made, the mode of deformation and fracture initiation behavior (Figure 18) were more similar to those observed in the test.

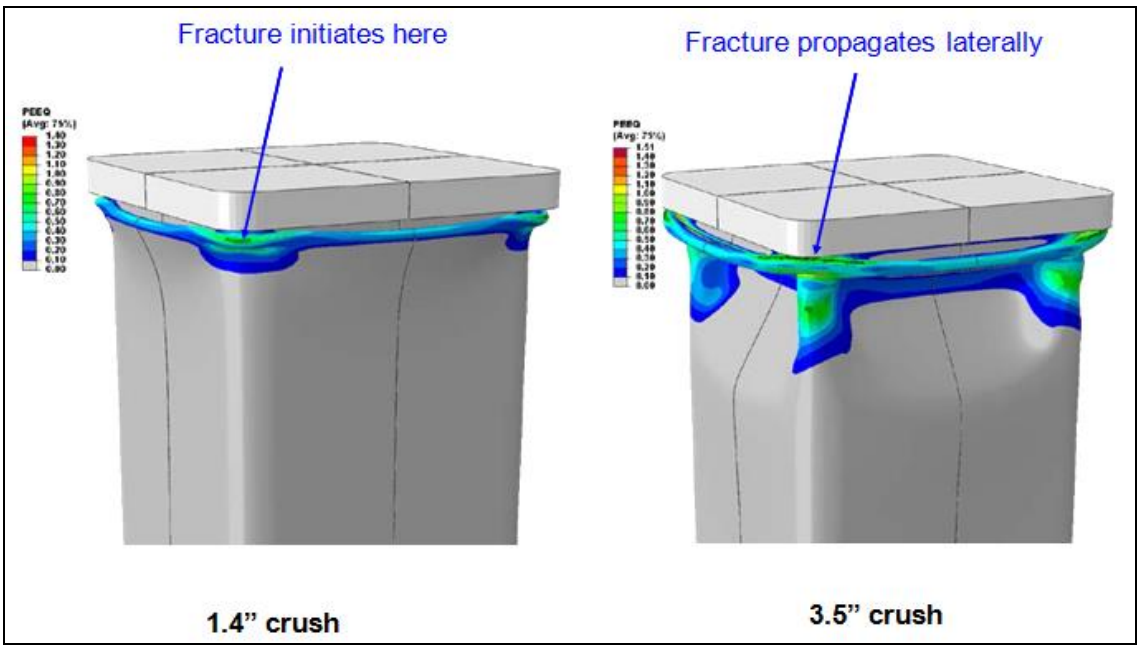

Figure 18. Contours of Equivalent Plastic Strain at 1.4" Crush (Just After Fracture Initiation) and at 3.5" of Crush
As predicted by a solid element-based model using Bao-Wierzbicki material failure model with fracture strain of 0.71.

3.2.6 Discussion

The results of the quasi-static tests clearly show that, while A572-50 steel appears to have excellent ductility, the slotted design of the crush tubes is not effective. The slot does serve to reduce the initial peak in load; however, it leads to failure of the A572-50 in the vicinity of the slot and, at least in the one crush test that was carried to completion, to complete separation of the top of the tube.

Post-test analysis indicates that this particular slotted design has a fundamental drawback: the slot is cut into the inside wall of the tube, all around the tube and including the corners. This causes the tube to mushroom outward in the slotted region as it crushes. The outward folding of the tube produces a large longitudinally-oriented tensile stress in the slotted region at the outside of the fold. In addition, because the tube is forced to deform outward, a large laterally oriented tensile stress arises in the corners of the tube, because the material needs to stretch to accommodate the larger radius of curvature of the outward-oriented fold. This creates a high level of triaxiality that promotes fracture in this region.

3.3 Subcomponent Crush Tests for Revised Tube Designs

Based on the test results, the slotted tube design was revised so as to remove regions of high triaxiality. Two alternative modifications to the design were evaluated, first with FEA and then with additional quasi-static tests. For both designs, the slots were cut only into the sides of the tubes, away from the corners. For one of the two designs, four slots were cut into the tube.

Slots were first cut into the inner surfaces of each of the opposing cut halves of the tube that would later be welded together to form the entire tube. Following welding, slots were cut into the outer surfaces of the tube, across each of the two weld lines. For the other design, only two slots were cut into the tube. In this case the slots were designed to cut only into the outer surface, one on each of the opposing non-welded sides. Both of these modified designs were thought to provide for more natural folding of the tube, i.e., without the extensive lateral stretching that occurs when the tube is forced to fold outward all around its cross-section.

A new crush tube, with the inside/outside four-slot pattern, was fabricated by BEPeterson. In addition, the second of the original crush tubes—which had been only partially crushed—was repaired by cutting off the crushed end to make a shorter (~14 inches long) tube. This tube had slots cut only into two opposing, non-welded sides of its outer surface. It was re-used because there was no more A572-50 material left from the same lot to make a new tube, and it was important to use material for the crush tubes from the same lot from which the deformable anti-climber test article crush tubes were being made.

On the newly fabricated tube with two inner and two outer slots (Figure 19a), the 1/8-inch deep slots are positioned 2.375 inches from the end of each tube. The slots were cut with a 1-inch diameter mill so as to limit stress concentrations along its edges. In the FEA model that was constructed to evaluate the crush behavior of this design (Figure 19b), solid elements were used to capture the geometry of the slots more accurately.

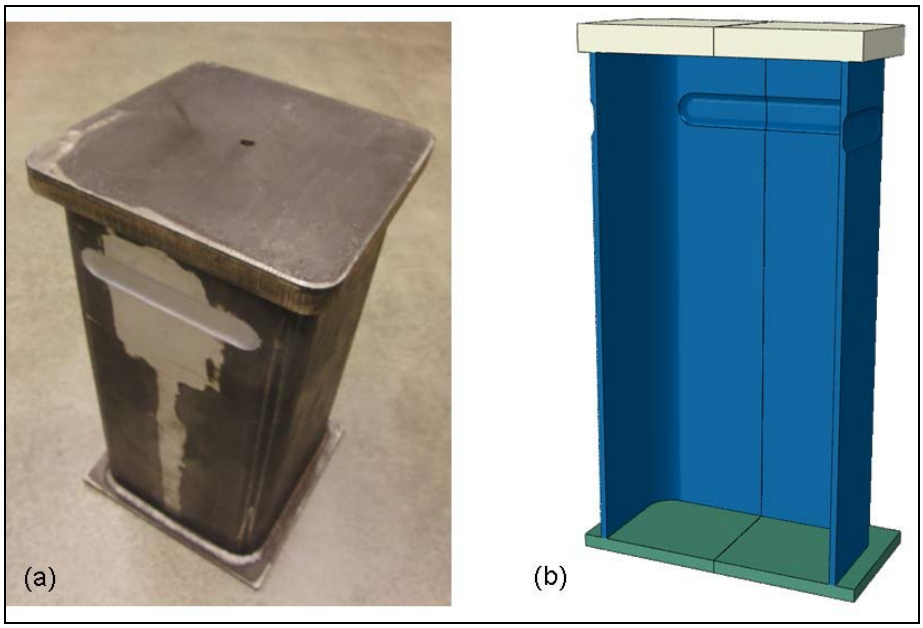

Figure 19. Photographs of Newly Fabricated Crush Tube and Design of Solid Element Based FEA Model
(a) Crush tube with revised slot design (two inside/two outside).
(b) Design of solid element-based FEA model showing internal and external slots.

3.3.1 Pre-test FEA

Pre-test FEA results indicate that these design changes decrease both the magnitude of the strains that arise during folding and the level of triaxiality, with only very local failure predicted to occur in unslotted portions of the tube as it folds (Figure 20).

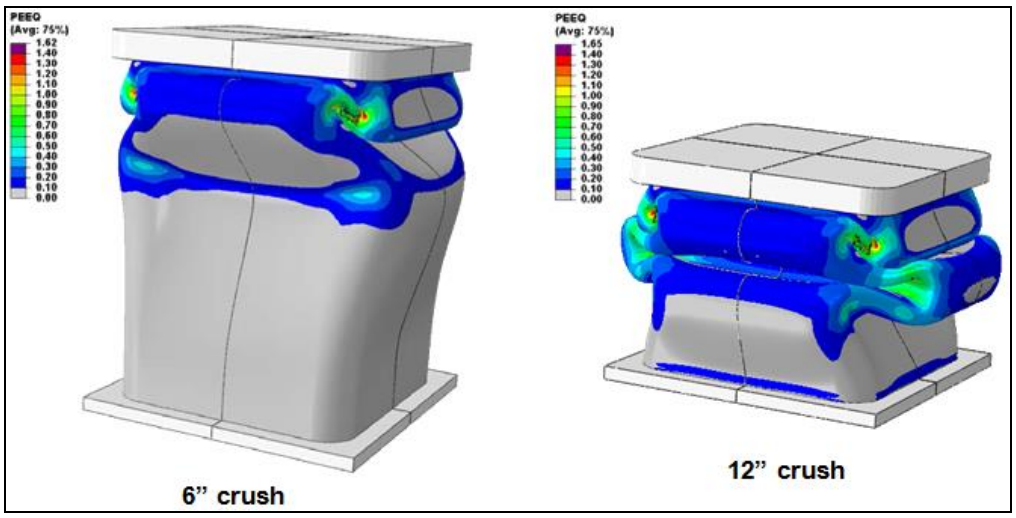

Figure 20. Predicted Deformation of Tube After 6" of Crush (left) and 12" of Crush (right) for Crush Tube with Two Internal and Two External Slots

3.3.2 Test Results

Figure 21 compares photographs of the deformed tube following the test with FEA predictions of the deformed shape. Clearly there is excellent agreement between the model and the test when the solid-based FEA model is used for this revised design. More importantly, the test results confirm that fracture is limited to very small regions in the corners of the tube, where the folding pattern is complex. There is no indication of any fracture modes that would lead to separation of tube components.

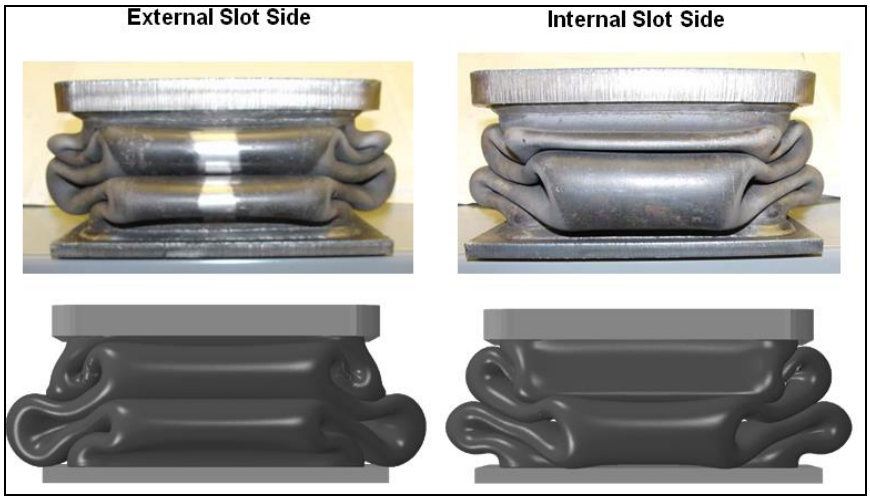

Figure 21. Comparison of Predicted Deformation vs. Actual Tested Deformation Following Test for Four-Slot Tube Design
Bottom: Predicted deformation. **Top:** Actual tested deformation (14.8" displacement.

Figure 22 compares the measured force-displacement curve with the FEA-predicted curve. Again, the agreement is excellent. The FEA model predicts the strain energy in the tube after 14.8 inches of displacement within 4% of the measured value.

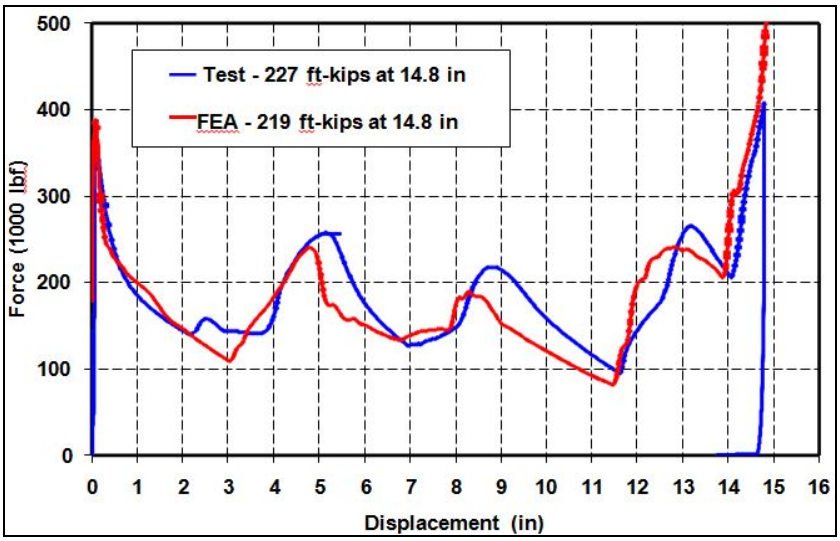

Figure 22. Comparison of FEA Predictions of Force-Displacement and Energy with Test Results for Four-Slot Tube Design

The crush behavior of the shorter, repaired, two-slot tube is similar to that of the longer, four-slot tube. The mode of deformation is similarly indicative of controlled folding, with limited fracture. Agreement with the FEA model is again very good (Figures 23 and 24). Note that, due to concerns about the peak load that would be exhibited by the two-slot design, the tube was crushed in two stages. In the first stage, the displacement rate was set to 0.25 inches per minute. Once the initial peak was determined, the load was removed and then reapplied at a displacement rate of 1.0 inches per minute.

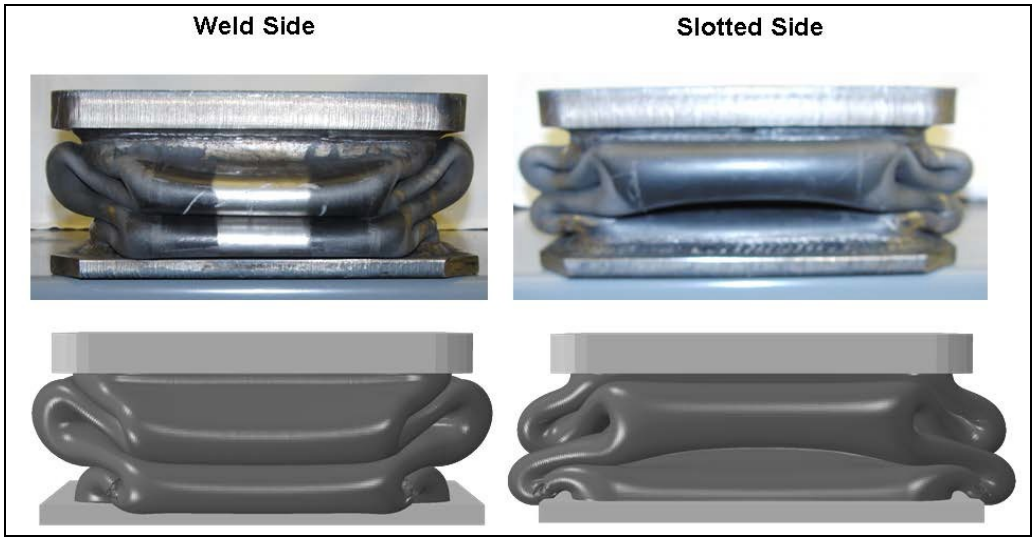

Figure 23. Comparison of Predicted Deformation vs. Actual Tested Deformation Following Test of Two-Slot Tube Design

Bottom: Predicted deformation. **Top:** Actual tested deformation (10.2” displacement.

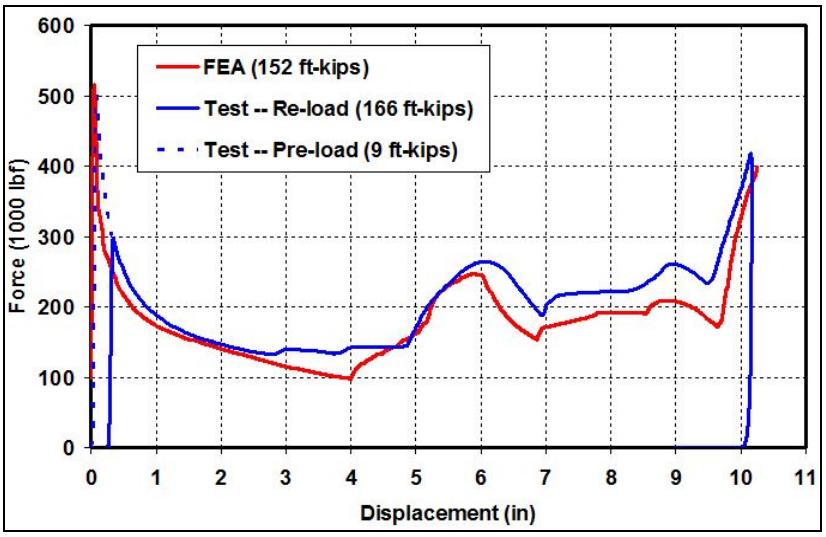

Figure 24. Comparison of FEA Predictions of Force-Displacement and Energy with Test Results for Two-Slot Tube Design

3.3.3 Discussion

In both cases above, the tube crush force-displacement behavior and mode of deformation were deemed to be acceptable as well as predictable. The key difference between the behaviors of the two tube designs is that the four-slot tube, because it has more material cut out of the tube, has a lower initial peak (385,000 lbf vs. 500,000 lbf for the two-slot tube). One of the requirements for the production deformable anti-climber system is to limit the maximum load (1,200,000 lbf for collision with a cab car and 1,600,000 lbf for collision with a freight car or locomotive), so that the structure behind the anti-climber does not collapse. The critical load arises when the second of the two sets of tubes is engaged in the collision, while the first set continues to collapse. The four-slot tube design was selected for the deformable anti-climber test article so as to limit the magnitude of the peak load associated with this second impact.

4. Fabrication and Quality Control

TIAX initiated test article fabrication by first soliciting quotes from two local metal fabricators: BEPeterson, in Avon, MA; and Vertex FD, in Middleton, MA. TIAX visited each of the fabricators and determined that both were fully capable of fabricating test articles of high quality. Detailed drawings of the test articles were provided to both companies so that they could assemble a quote. BEPeterson was ultimately selected, based on price and a reputation for maintaining excellent communication with clients throughout projects.

Following their selection as fabricator, TIAX visited BEPeterson to review issues with respect to the drawings. BEPeterson marked a few changes to drawings, mostly to deal with tolerances or to make changes to pre-machining dimensions of certain components that required post-weld finish machining.

TIAX assembled a quality control document to guide the test article fabrication. In addition to BEPeterson's own internal quality control procedures, TIAX agreed with BEPeterson to designate "hold points" for the push-back coupler test article, where TIAX personnel could visit BEPeterson and inspect the two key test article assemblies before final welding and machining. The two hold points were:

- *Coupler test fixture assembly:* After fit and tack of the entire unit prior to welding according to notes 1-5 on welding and assembly sequence provided with drawing TC09016-0023
- *Sliding lug assembly:* After fit and tack of entire unit prior to welding and machining according to drawing TC09016-0027.

TIAX personnel visited BEPeterson in September 2011 to inspect the tack-welded main assemblies. A large number of key dimensions were measured and found to be within drawing tolerances. In general, TIAX had a very favorable impression of BEPeterson's work. Figures 25, 26, and 27 show photographs of the support beam assembly, the side wall assembly, and the sliding lug assembly, respectively, taken during the inspection. The support beam assembly (Figure 25) was in the process of final welding; the other two assemblies were tack-welded and awaiting final welding.

Figure 25. Support Beam Assembly Undergoing Final Welding

Figure 26. One of Two Side Wall Assemblies Before Final Welding

Figure 27. Sliding Lug Assembly Before Final Welding

BEPeterson completed fabrication of all of the push-back coupler test article assemblies, except for final machining and installation of the shear bolts, in November 2011. TIAX and Volpe personnel made an inspection visit to BEPeterson shortly thereafter. A number of key dimensions were measured and found to be in tolerance. Photographs taken during that visit are shown in Figures 28 and 29.

Figure 28. Photographs of the Push-Back Coupler Test Article, Minus the Sliding Lug Assembly

Figure 29. Photograph of the Sliding Lug Assembly Before Final Machining

BEPeterson shipped the push-back coupler test article, including the sliding lug, to a machining specialist who performed the final machining of the sliding lug and installed the shear bolts. The shear bolts had been received by TIAX from Voith (who designed and manufactured them) and forwarded to BEPeterson. As part of the quality control process, the ability of the lug to slide backward into the support assembly was verified (Figure 30). (Note that assembly is upside-down.)

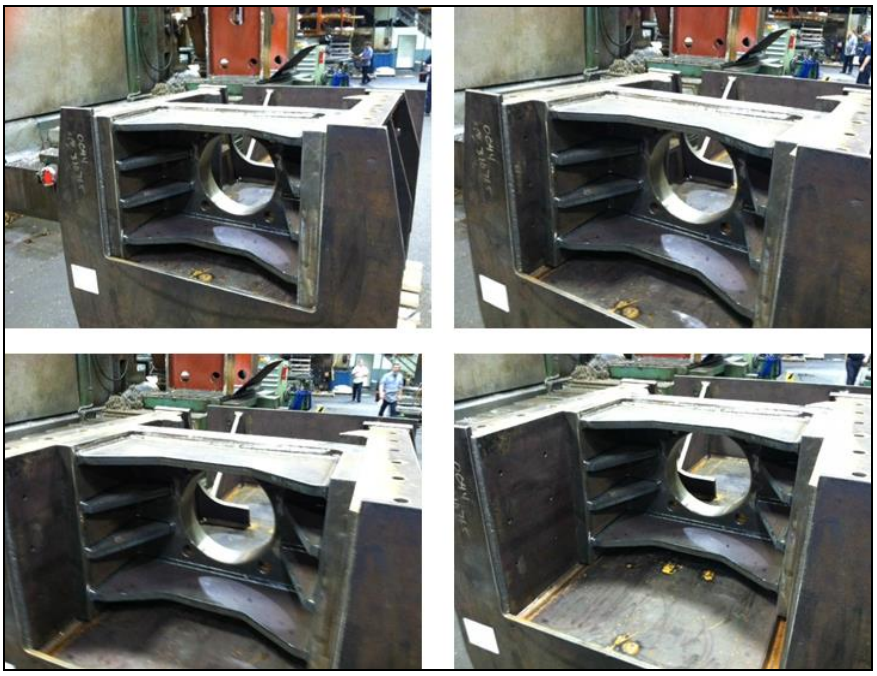

Figure 30. Photographs Showing Push-Back of Sliding Lug After Final Machining of Side Walls

One small issue was encountered: when the lug was positioned in its most forward location, there was slight interference between the top edge of the side walls of the lug and the weld between the front plate of the assembly and the side plates. Due to the interference, there was a small gap (approximately 0.25 inches) between the front of the lug and the rear of the front plate. It was agreed that this would be corrected by adding a 0.375-inch by 45-degree chamfer to those edges of the lug. It was also agreed that a similar chamfer would be added to the laterally oriented top back edge of the sliding lug to further minimize the potential for binding (Figure 31).

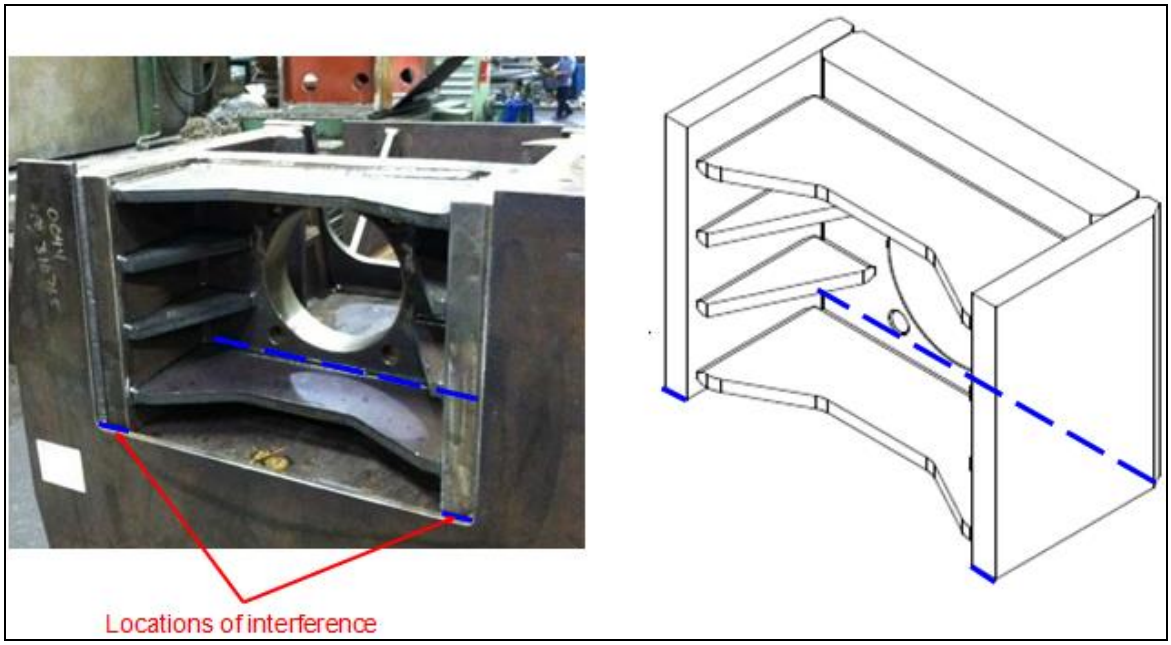

Figure 31. Photograph and Schematic Illustration of Sliding Lug

Photograph (left) and Schematic Illustration (right) show two locations of interference that required chamfering, plus an additional edge on the rear of the lug where a chamfer was added to minimize potential for binding.

It was further agreed that a 0.03-inch shim would be placed between the lug and the bottom plate of the support assembly (which is underneath the lug in its upside-down configuration) during drilling for and installation of the shear bolts. Finally, it was agreed that the bottom surface of the lug would be ground so that there would also be approximately 0.03 inches of clearance between it and the "rail stopper" plates that are bolted to the underside of the side wall assemblies to support the lug during push-back.

These modifications were made, and the shear bolts were installed. The complete assembly was then returned to BEPeterson for final inspection and preparation for shipping. In January 2012, a final inspection visit was made by TIAX and Volpe personnel at BEPeterson. Photographs of the completed test articles (Figures 32 and 33) were taken at BEPeterson. Additional measurements were made of key test article features, particularly the gaps between the sliding lug assembly and the support assembly, which were found to be within tolerance.

Figure 32. Photograph of Completed Deformable Anti-climber Test Article

Figure 33. Photograph of Completed Push-Back Coupler Test Article (Upside Down)

The test articles were picked up from BEPeterson by Wetmore Co. and taken to their facility in Wilmington, MA, for crating (Figures 34 and 35). Once crating was completed, the test articles were delivered to NNR Logistics, the company responsible for shipping, and were prepared for shipping. NNR worked with the test facility, TÜV SÜD, to sort out the logistics of the shipment, including the waiver of Value Added Tax (VAT). Volpe supported this effort by providing a letter describing the test articles as government property that would be used for testing.

Figure 34. Photographs Taken During Crating of Deformable Anti-Climber Test Article

Figure 35. Photographs Taken During Crating of Push-Back Coupler Test Article

5. Component Tests

This section describes the procedures and results of the dynamic tests of the two crashworthy components. The purpose of the tests was to verify certain performance characteristics of the components and to provide information for comparison to FEA model predictions. The tests were conducted on April 4th and 5th, 2012. Both tests were witnessed by Rich Stringfellow (TIAX), Ron Mayville (SGH), and Kari Jacobsen (Volpe). Tony Jones and Thomas Ewerding of Voith witnessed the push-back coupler test.

5.1 Test Facility

Dynamic testing was conducted at TÜV SÜD Rail GmbH, in Görlitz, Germany (Figure 36) under contract to TIAX's subcontractor, SGH. The Görlitz facility is an accredited test laboratory pursuant to DIN EN ISO/IEC 17025 for the tests described in this document. Furthermore, TÜV SÜD Rail GmbH is accepted for approval testing of railway vehicles by the German Federal Railway Authority (Eisenbahn-Bundesamt) and by several certified bodies throughout the European Union.

Figure 36. Görlitz Dynamic Test Facility

5.2 Test Implementation Plan

A test implementation plan prepared by SGH was reviewed and approved by Volpe (with a few modifications) prior to the test. Some of the key details of the plan are included in the following sections.

5.2.1 Impact Vehicle

The impact energy for both tests was provided by a moving rail car (Figure 37) with mass equal to 79.8 tonnes (176,000 lbm), brought to the test collision speed by a V22 locomotive (Figure 38). The locomotive pushes the impact car to a speed just greater than the desired test speed and releases it a few hundred meters before the test wall. The condition of the front plate of the impact car depends on the test. For the push-back coupler test, the test article was mounted to the flat, forward end of the vehicle. For the deformable anti- climber test, the test article was mounted to the instrumented wall and impacted by the flat end of the vehicle.

Figure 37. 80-Tonne Impacting Rail Car Used for Both Tests

Figure 38. The Pushing Locomotive, Type V22

The suspension system of the impacting rail car was modified prior to the test due to concerns about possible pitching motion. TÜV SÜD added bolts to the impacting rail car to limit the travel of the car body relative to the truck. Figure 39 shows an example. A bolt was installed at each of

the four suspension spring locations of the front truck only. The head of the bolt was turned to make contact with the plate on the spring in each case just prior to the tests.

Figure 39. Photographs of One of the Bolts Used to Limit Vertical Travel of the Car Body With Respect to the Truck

5.2.2 Instrumented Impact Wall

The impact wall consists of a thick steel plate mounted on a concrete base (Figure 40). Load cells are mounted onto the plate in a configuration that depends on the test.

Figure 40. End Platform Plate on the Impact Wall

For the deformable anti-climber test, the test article was mounted to the instrumented impact wall, as described Section 5.5.

5.2.3 Instrumentation

The instrumentation used in the dynamic testing was nearly the same for both tests and so is described in this section. Table 3 lists the general approach to measuring various parameters. The instruments were calibrated in accordance with accepted standards of practice.

Table 3. Instrumentation Used for the Component Tests

Parameter	Instrumentation Approach	Tests
Load	Load cells on the test wall	Push-back coupler, deformable anti-climber
	Load cell on the end of the dummy coupler	Push-back coupler
Displacement	Ruled strip on the side of the impacting rail car	Push-back coupler, deformable anti-climber
	String pot	Push-back coupler
Impact speed	Photo sensors on the ground	Push-back coupler, deformable anti-climber
Video	High speed digital cameras above and to the side	Push-back coupler, deformable anti-climber
	Conventional video	Push-back coupler, deformable anti-climber
Accelerations	Accelerometers mounted to the rail car	Push-back coupler, deformable anti-climber

Load and Displacement

The loads were recorded by load cells mounted on a plate on the impact wall. The push-back coupler test configuration consisted of four load cells mounted in a square pattern (Figure 41). The deformable anti-climber test load cell configuration consisted of six load cells with two groups of three cells mounted in an equilateral triangle pattern (Figure 42). The characteristics of the load cells are listed in Table 4.

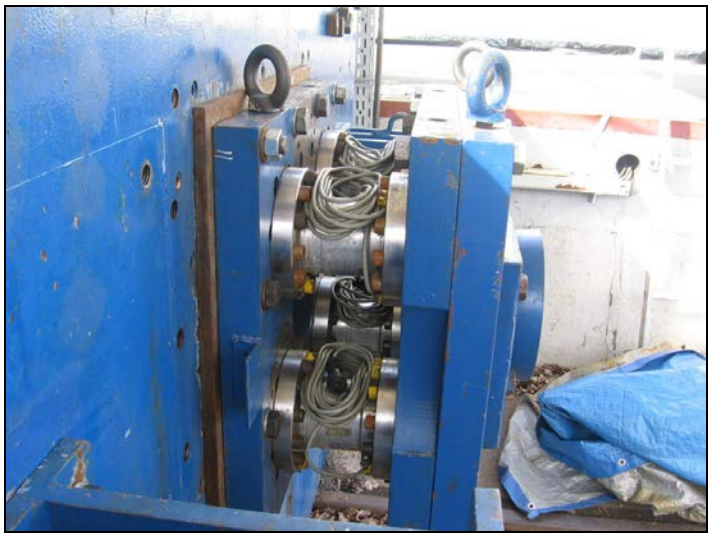

Figure 41. Load Cell Configuration on the Impact Wall Used for the Push-Back Coupler Test

Figure 42. Load Cell Configuration on the Impact Wall Used for the Deformable Anti-Climber Test
The target on the right angle support plate was used for focusing the camera and was removed prior to the test.

Table 4. Instrumentation Used to Measure Load and Displacement

Instrument	Type	Manufacturer	Model	Range	Quantity	Test
Load cell	Strain gage	HBM GmbH	Special	2 MN	4	Push-back coupler
				1.2 MN	6	Deformable anti-climber
Ruler	Laser	TUV	Special	2.5 m	1	Both
String pot	—	ASM Moosinning	WS10-1250-HG	—	1	Push-back coupler

The primary displacement measurement system, used for both tests, consisted of laser sensors that read a ruled strip mounted on the side of the impacting rail car, as illustrated in Figures 43 and 44. This system has been found to be very accurate. A string potentiometer was also used to measure displacement for the push-back coupler test. (The details of this instrumentation are listed in Table 4.) The data signals were amplified through signal conditioners and recorded using an MGCplus with Quantum X amplifier modules, manufactured by HBM GmbH, and a measuring computer. After the test, the data were downloaded to a dedicated data-acquisition computer in a digital format. Data were subsequently processed using PC-based computer programs. The gradation of the laser/ruler displacement measurement system is 2.5 mm.

Figure 43. Stroke Measurement by the Laser/Ruled Strip

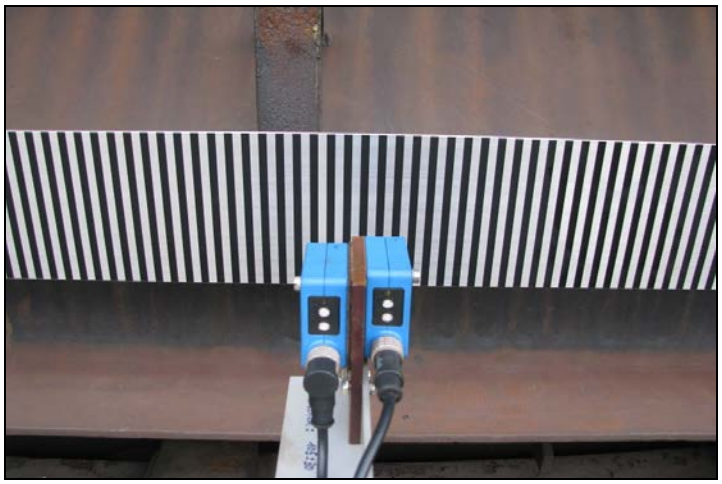

Figure 44. Ruled Strip Stroke Measurement System Close-up

Acceleration

Six accelerometers were mounted onto the impact rail car for both tests. There were two sets of three accelerometers. Each set consisted of one accelerometer in each of the three directions: longitudinal, vertical, and lateral. The two sets were mounted on the same (left) side of the car, one at the front and one at the rear (Figure 45). Figure 46 shows a photograph of the front accelerometer set. The accelerometers are manufactured by HBM, models B12/200 and B12/500. The characteristics of each of the individual accelerometers are listed in Table 5.

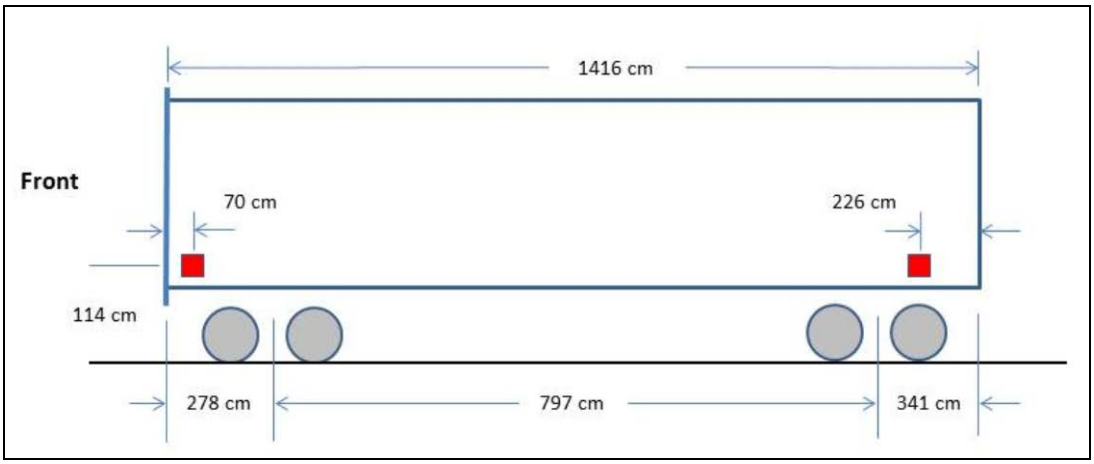

Figure 45. Positions of Accelerometer Sets on the Impact Rail Car

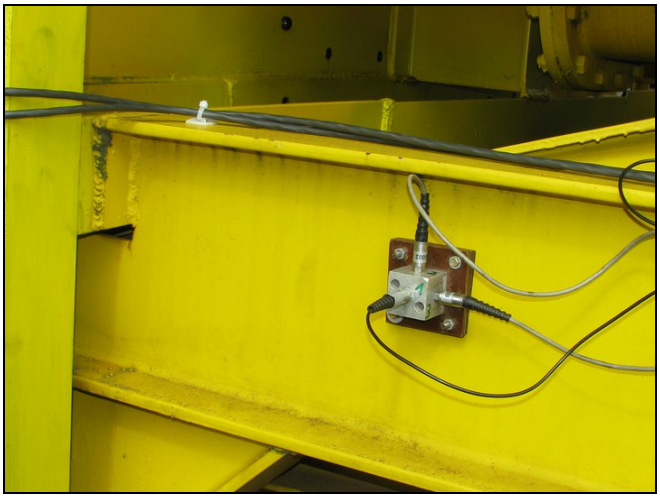

Figure 46. One of the Accelerometer Sets Mounted to the Impact Rail Car

Table 5. Accelerometer Information

Sensor ID	Location	Orientation	Model
a1	Front	Lateral	B12/500
a2	Front	Vertical	B12/200
a3	Front	Longitudinal	B12/500
a4	Rear	Lateral	B12/200
a5	Rear	Vertical	B12/200
a6	Rear	Longitudinal	B12/500

5.2.4 Photographic Documentation

Two high-speed cameras and one regular video camera were used to record each of the tests. Synchronization and triggering were accomplished by a laser detection system mounted at the side of the track. The characteristics of the cameras used for the tests are shown in Table 6. The locations of the cameras were different for the two tests (Figures 47 and 48).

Table 6. Photographic Equipment Used for the Tests

Type	Manufacturer	Model	View Location
Real-time video	--	DV	Straight on, overall view
High-speed video	Weinberger	SpeedCam MacroVis	Side
High-speed video	Weinberger	SpeedCam MacroVis	Front or top
Digital-still-camera	Canon	S5	Various positions, before and after the test

Figure 47. Locations of High-Speed Cameras for Push-Back Coupler Test

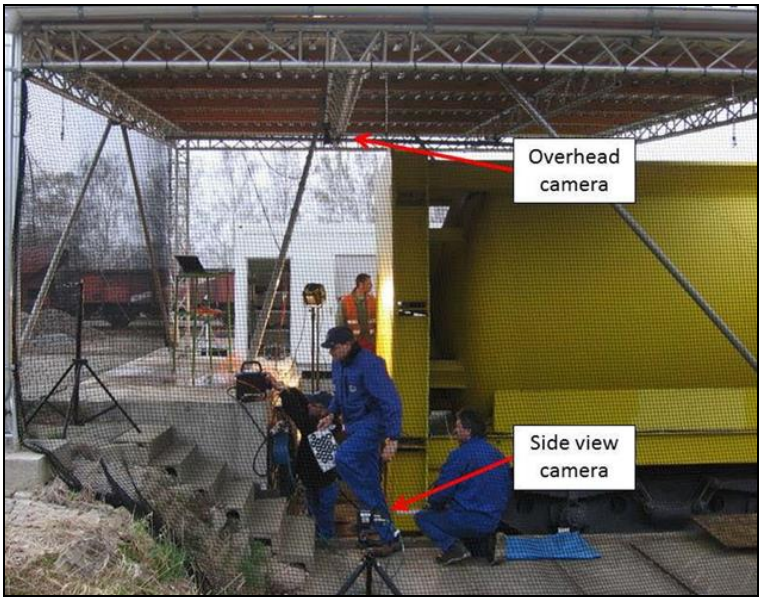

Figure 48. Locations of the High-Speed Cameras for Deformable Anti-Climber Test

5.2.5 Speed Measurement

The speed measuring system (Figure 49) was a GME (Railmotive Görlitz) with two reflection photo sensors at a distance of 19.7 inches (50 cm). The speed is calculated from the time interval

measured, scanning by means of two reflection photo sensors with 90° phase shift to identify the direction of motion and the reversal point.

Figure 49. Speed Measurement by Means of Photo Sensors

5.3 Pre-test Calculation

The target impact speeds were calculated for each test so as to meet the requirements of the test without damaging test equipment. FEA predictions of the outcomes for the two tests were made and were included as an addendum to the test implementation plan.

5.3.1 Impact Speed Range

A range of acceptable impact speeds was calculated for each test, based on the energy requirements for the test article and other aspects of the test, including safety of the instrumentation. Note that, as is discussed in this section, the target impact speed for the push-back coupler test was modified on the day of the test due to limitations in the possible stroke of the residual energy absorbers.

Push-Back Coupler Test Article

For the push-back coupler test article, the minimum impact speed was selected first so as to ensure that the full stroke of the deformation tube is exhausted and the bolts shear off. For impact speeds that are higher than is required to break the bolts, the residual kinetic energy is absorbed by four energy-absorbing buffers, with a rated total capacity of 1,600 kJ (1,180 ft-kips).

The deformation tube load is designed to build up linearly over ~3 inches of displacement and then remain constant at 674,400 lbf for a stroke of 15 additional inches until a feature built onto the back of the surrogate coupler shank impacts the front face of the mounting block of the deformation tube assembly (see Figure 3). This provides an energy of 11,130 in-kips. Assuming the bolts break at a constant force of 1,056 kips over a distance of 0.25 inches, this adds an extra 260 in-kips, bringing the total energy to 11,390 in-kips (950 ft-kips).

A 20% “safety margin” was added to this energy value in order to ensure that there would be more than enough energy to exhaust the stroke of the push-back coupler and fail the shear bolts at the minimum impact speed. When this 20% margin is added, the minimum desired kinetic energy of the impacting vehicle is E =13,670 in-kips. For a total vehicle mass M of 182,600 lbm (176,000 lbm for the car + 6,600 lbm for the test article), the minimum acceptable impact speed can be calculated as:

$$V_o = \sqrt{2*E_k/(M/g)} = 241 \text{ in/sec or } 22 \text{ km/hr} \quad ,$$

where *g* is acceleration of gravity (386.4 in/sec).

The test facility is able to guarantee an impact speed range of ±2 km/hr. Therefore, the nominal impact speed is set to 24 km/hr (262 in/sec), and the maximum impact speed is set to 26 km/hr (284 in/sec).

The calculated kinetic energy for the nominal impact speed is 15,810 in-kips (1,320 ft-kips), thus the expected residual energy is (15,810-11,390) = 4,420 in-kips (370 ft-kips). At the maximum impact speed, the calculated kinetic energy is 18,620 in-kips (1,550 ft-kips), and the residual kinetic energy is 7,230 in-kips (600 ft-kips). This is well below the rated capacity of the residual energy absorption buffers.

(It should be noted that, prior to the test at the test site, an issue with this pre-test calculation was identified. Because of the desire to have the shear bolts fail prior to engaging the residual energy buffers, the buffers were set up to begin absorbing energy approximately 3 inches past the point at which the bolts were loaded. To prevent the sliding lug from exiting out the back of the draft pocket during the crush sequence, a stop was built into the draft pocket that limited the motion of the sliding lug to 14 inches, leaving 11 inches of residual buffer stroke before the draft pocket stroke was exhausted. Based on the load-displacement characteristics of the four buffers, it was determined that it was not possible to achieve the full capacity of the buffers. Because of this, the nominal impact speed was lowered from 24 km/hr to 23.5 km/hr in order to protect the load cells from a spike in load that would accompany bottoming out of the draft pocket. This effectively lowered the minimum acceptable speed range to 21.5 km/hr, which corresponds to a kinetic energy of 13,020 in-kips, and reduces the margin at the low end of the range from 20% to 14.3%. As discussed in Section 5.4 below, the actual impact speed was well below the minimum impact speed, due to a number of factors.)

For the deformable anti-climber test article, there are no supplemental energy-absorbing buffers. Therefore, the maximum impact speed was calculated so that the instrumentation would not be damaged due to build-up of load accompanying consolidation of the crushed tubes. The target maximum acceptable load was selected as 1,500 kips during the initial stages of consolidation. As is discussed in the following section, pre-test FEA calculations indicate that a load of 1,500 kips will arise after 16.0 inches of deformation. The deformation energy at this displacement is 13,640 in-kips (1,140 ft-kips), and the maximum impact speed is thus calculated as:

$$V_o = \sqrt{2*E_k/(M/g)} = 241 \text{ in/sec or } 22 \text{ km/hr} \quad .$$

Thus, for the guaranteed speed range of ±2 km/hr. the nominal impact speed is 20 km/hr, and the minimum impact speed is 18 km/hr. The kinetic energy associated with the nominal impact speed is 11,020 in-kips (920 ft-kips). The predicted crush for an equivalent extent of deformation energy is 13.5 inches. At the minimum speed of 18 km/hr, the kinetic energy is 8,930 in-kips (740 ft-kips), and the predicted extent of crush is 10.9 inches.

5.3.2 Pre-test FEA

Prior to the tests, simulations of each test were performed using ABAQUS/Explicit. The results of these analyses are detailed in the final report for the Base Effort of this program [20]. Due to changes in the design of the deformable anti-climber crush tubes, a new FEA model was constructed and analyzed for this test article. Pre-test predictions of performance for both test articles are described below.

Deformable Anti-Climber

Pre-test predictions of the force-displacement curve and the associated modes of deformation for the deformable anti-climber test were calculated through the FEA model (Figure 50), which has approximately 600,000 elements and is symmetric about a vertical-longitudinal plane. The deformable anti-climber structures are modeled with shell elements, with the characteristic element size ranging from 0.0625 inches in the crush tubes to 0.125 inches in the other structures. The back plate was modeled as rigid.

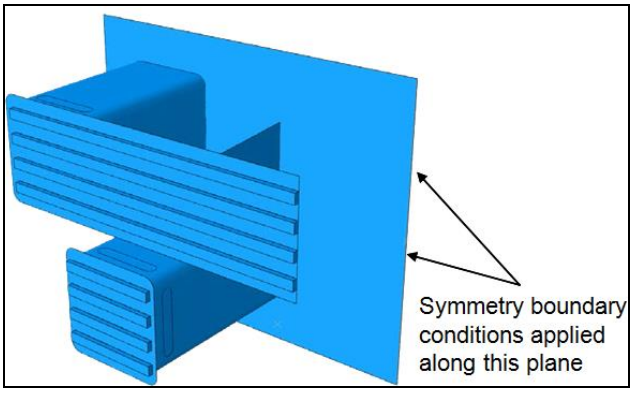

Figure 50. FEA Model of the Deformable Anti-Climber Test Article
Flat rigid surface representing the impacting surface is not shown.

In order to better mimic the geometry of the slots, inside or outside perturbations in the geometry of the tube were introduced at the slot locations, with a peak magnitude of 0.0625 inches (one-half the magnitude of the decrease in thickness associated with the slot, since shell elements were used). In addition, a smoothly varying decrease in the thickness of the elements in the slot was introduced using the *DISTRIBUTION feature of ABAQUS.

The material failure model that was developed for simulating the subcomponent crush tests (Section 3.2.5) was implemented in ABAQUS, using failure parameters that were validated through comparison with the results of the quasi-static tests. The impacting vehicle was represented as a moving rigid flat wall with mass equal to that of the impact vehicle (176,000 lbm).

The predicted final displacement and energy absorption levels for the minimum, nominal, and maximum impact speeds are indicated in Figures 51 and 52. The predicted force-displacement curve is shown in Figure 51. The load is expected to rise to 680 kips shortly after impact of the vehicle with the two lower crush tubes, then drop to 300 kips during the first two inches of crush, and then rise to 1,460 kips as the flat wall of the vehicle impacts the plate that connects the two upper crush tubes. An analysis of model results suggests that the initial stiffness of the angled

plates contributes significantly to this second peak in load. The magnitude of the load then undulates as the tubes fold, until the deformation reaches about 15 inches, at which point the tubes consolidate, and the load builds sharply. The associated energy versus displacement curve is shown in Figure 52. The modes of deformation corresponding to these levels of crush are shown in Figures 53, 54, and 55 for the three indicated impact speeds.

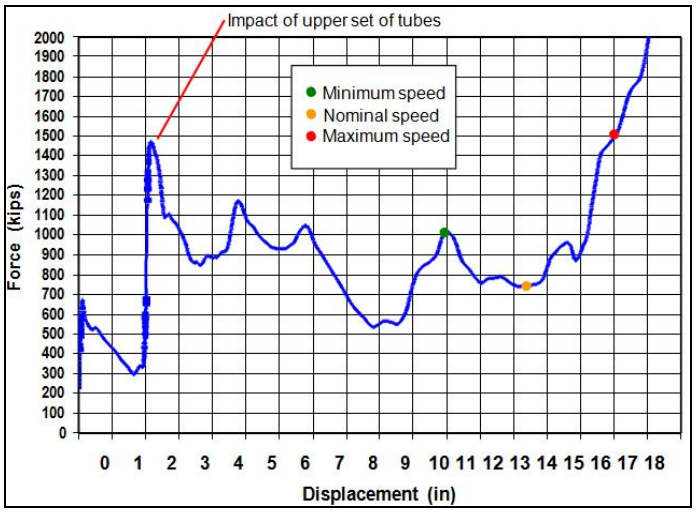

Figure 51. Predicted Force-Displacement Curve for Anti-Climber Test Article
Predicted final force/displacement for different impact speeds is indicated.

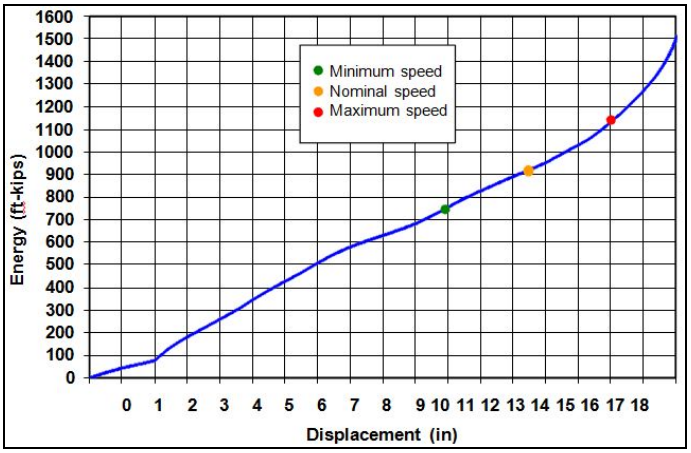

Figure 52. Predicted Energy-Displacement Curve for Anti-Climber Test Article
Predicted final energy/displacement for different impact speeds is indicated.

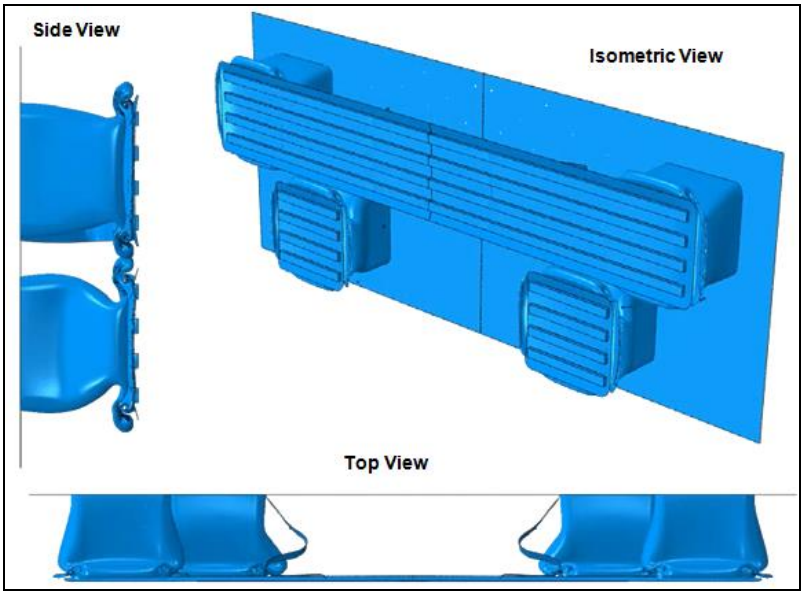

Figure 53. Predicted Shape of Deformed Test Article Corresponding to Minimum Speed (18 km/hr) Impact (10.9 Inches Crush)

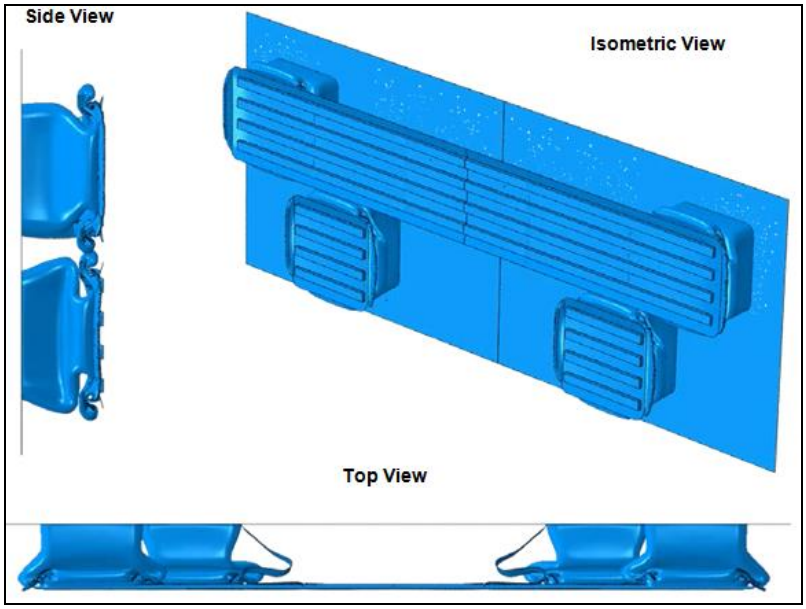

Figure 54. Predicted Shape of Deformed Test Article Corresponding to Nominal Speed (20 km/hr) Impact (13.5 Inches Crush)

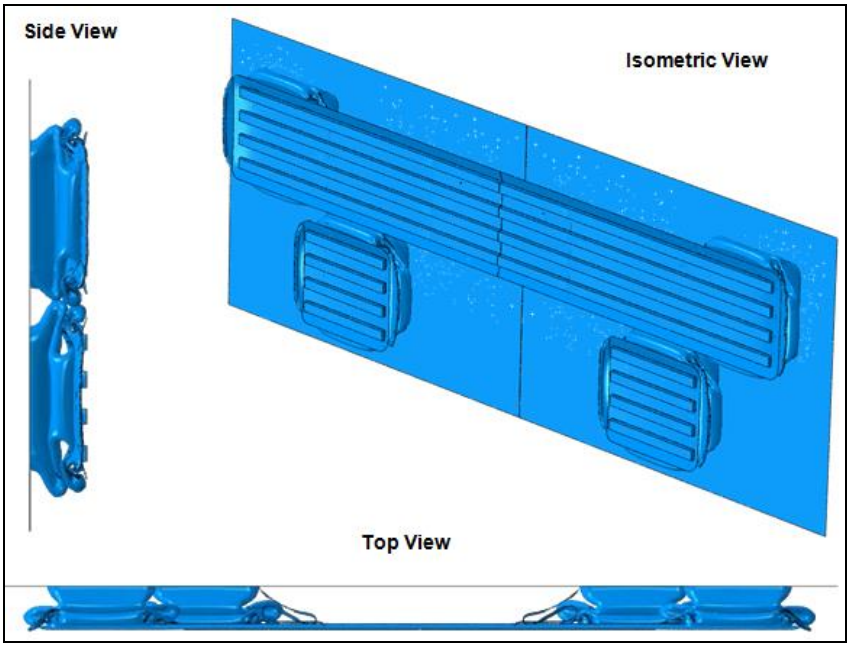

Figure 55. Predicted Shape of Deformed Test Article Corresponding to Maximum Speed (22 km/hr) Impact (16.0 Inches Crush)

Push-back Coupler Test Article

The complexity of the design of the deformation tube-based push-back coupler and the shear-bolt fuse mechanism makes it challenging to model the load-deformation characteristics of these structures in detail. Instead, they were modeled with more simplified elements whose behavior is determined largely on the basis of the value of pre-defined parameters. For this reason, pre-test predictions for the force-displacement response of the push-back coupler test article are based largely on design curves for the deformation-tube force-displacement response and on the design strength of the shear bolts.

An FEA model prediction of the impact was made using connector elements to model the deformation tube crush and shear bolt failure. The model is shown in Figure 56. Predictions of force-displacement taken from the model are shown in Figure 57. For various reasons associated with the simple manner in which deformation tube and shear bolt characteristics are defined, the model predicts a level of dynamic excitation during push-back that, based on previous test results, is unlikely to be so great in the actual test. For this reason, the response that would be predicted solely on the basis of the design curve for the deformation tube and the design capacity of the shear bolts (see Figure 5) is plotted for comparison.

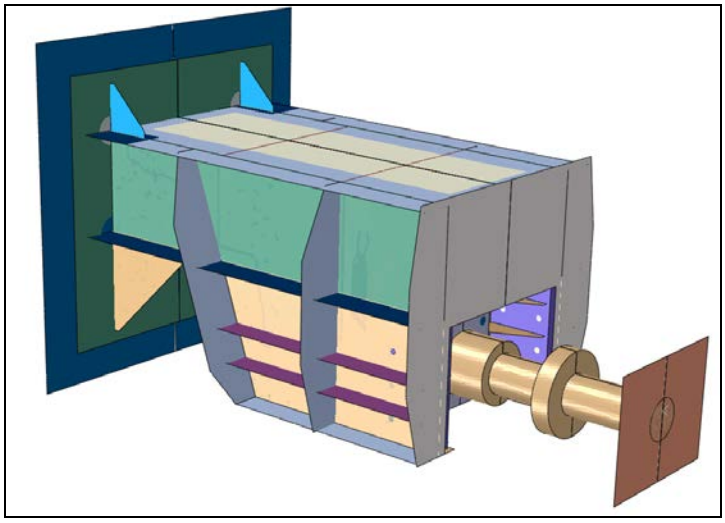

Figure 56. FEA Model for the Push-Back Coupler Test Article

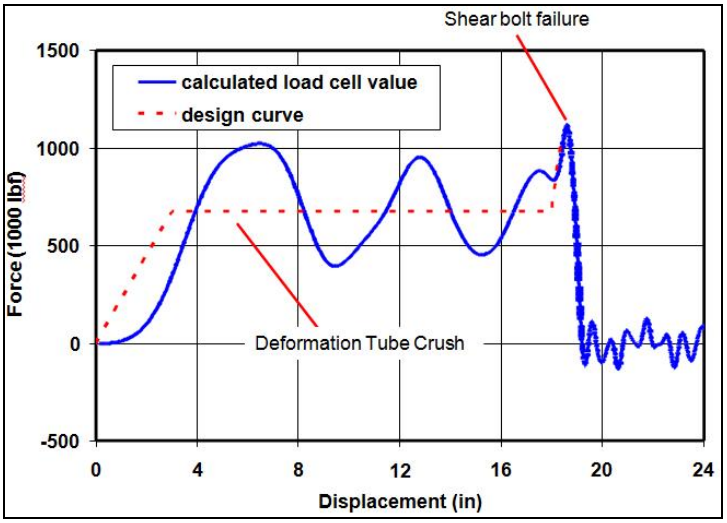

Figure 57. Calculated Force-Displacement Behavior for Push-Back Coupler Test Article
Push-back coupler design curve is indicated for reference.

5.4 Push-back Coupler Test Description and Results

5.4.1 Test Description

Figure 58 shows an illustration of the test configuration for the push-back coupler test. Figure 59 shows a photograph of the test article, which is mounted to the impacting rail car and has an extension component that represents an actual coupler shank. There is a load cell mounted on the end of this extension piece (Figure 60), which impacts the end plate of the test wall load cell system within a ring that prevents lateral motion.

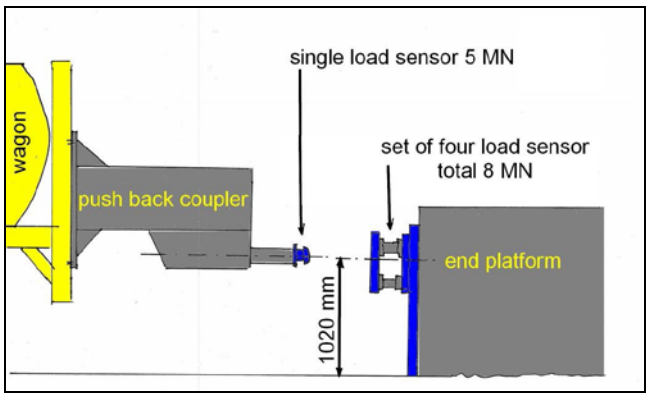

Figure 58. Illustration of the Push-Back Coupler Configuration

Figure 59. Photograph of the Push-Back Coupler Test Article Mounted on the Impact Car

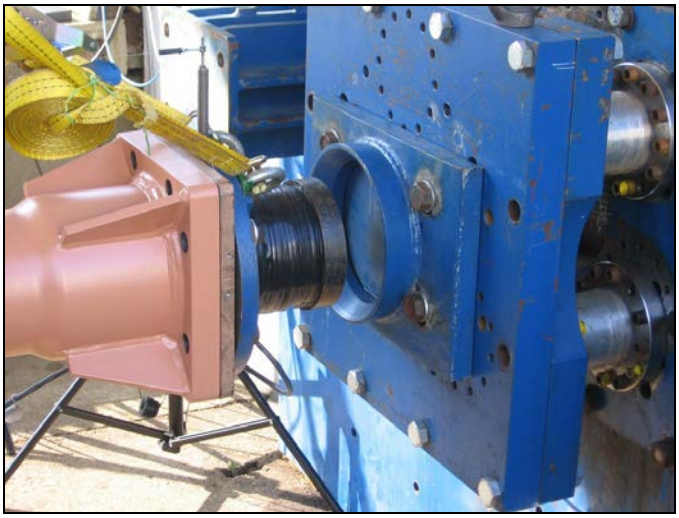

Figure 60. Photograph Showing Interaction of the Push-Back Coupler Extension Piece With Load Cell and End Plate of the Wall-Mounted Load Cell System

The extension piece normally is not restricted from rotating about the coupler pin. It was supported both vertically and laterally by straps to prevent it from moving significantly before impact (Figure 61). The straps did not interfere with the push-back motion of the extension and coupler. Energy absorbing buffers were mounted on the sides of the test article on both the rail car and the crash wall to absorb residual energy should such absorption be required.

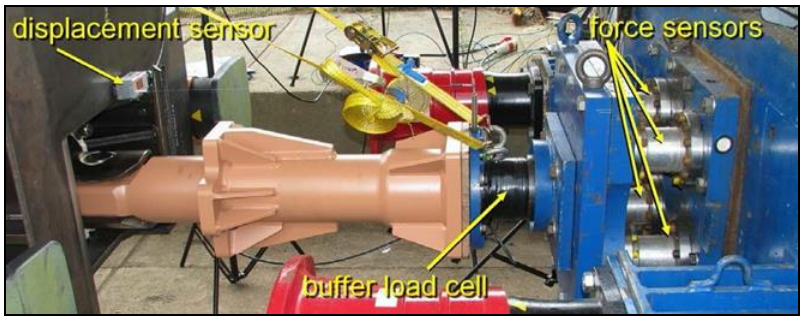

Figure 61. Photograph Showing Supporting Straps for the Push-Back Coupler Extension Piece
The "buffer load cell" is attached to end of the push-back coupler.

Two impacts were required to complete the push-back coupler test. Due to an error made by the test facility personnel (having to do with changes that were made to the suspension system of the impact vehicle), the speed of the rail car in the first impact was 19.9 km/hr (12.4 mph), which was well below the target impact speed of 23.5 km/hr and the minimum guaranteed impact velocity of 21.5 km/hr. Because the initial kinetic energy associated with this impact speed (10,800 in-kips) was slightly less than the energy required to exhaust the deformation tube (11,130 in-kips), there was insufficient energy to fail the shear bolts. For this reason, a second impact was conducted, with a target speed (6.8mph = 11 km/hr) chosen to provide enough energy to exhaust the remaining deformation tube stroke (approximately 3 inches) and completely fail the shear bolts. For this second impact, the measured impact speed was 7.4 mph (11.9 km/hr). The shear bolts all failed, and the sliding lug moved approximately 10 inches into its pocket.

5.4.2 Test Observations and Results

Figures 62 and 63 show the test article after the first impact. The deformation tube was essentially exhausted. Lubrication ports that extended outward about ½ inch from the coupler mounting block were partially crushed, indicating that the back plate of the coupler extension had just made contact in the first impact. This was consistent with the 18-inch stroke measured for this part of the test.

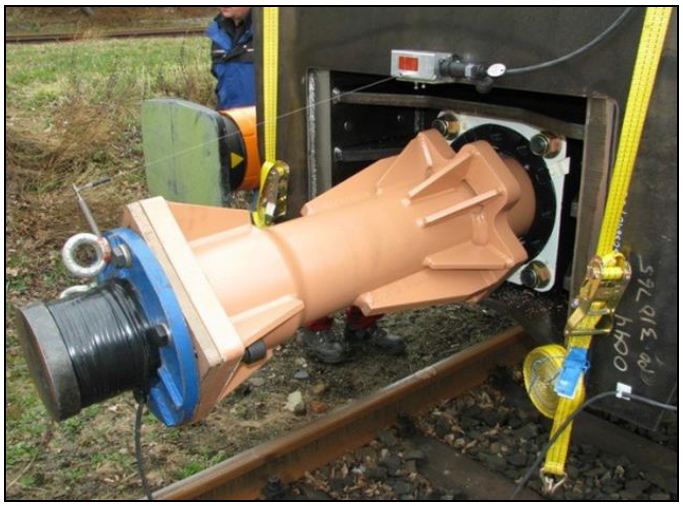

Figure 62. Push-Back Coupler Test Article After the First Impact

Figure 63. Push-Back Coupler Deformation Tube After the First Impact

Two independent measurements of impact load were made for this test. Figure 64 compares measured load-displacement responses for the load cell set mounted on the instrumented wall with the single load cell mounted at the end of the coupler extension (see Figure 60). The two measures of load are generally consistent. Figure 65 shows measured raw and filtered load versus displacement, with the load in this case taken from the load cell set on the wall. In both figures, the displacement is taken from the ruled strip until a maximum displacement is reached, then taken from the string potentiometer at the coupler extension, which properly shows the rebound effect (which the ruled strip does not). Note that the data in Figure 65 have been filtered with CFC 60, because filtering with CFC 180 shows significant fluctuation in load at low displacement (Figure 66), which makes it difficult to identify the push-back trigger load.

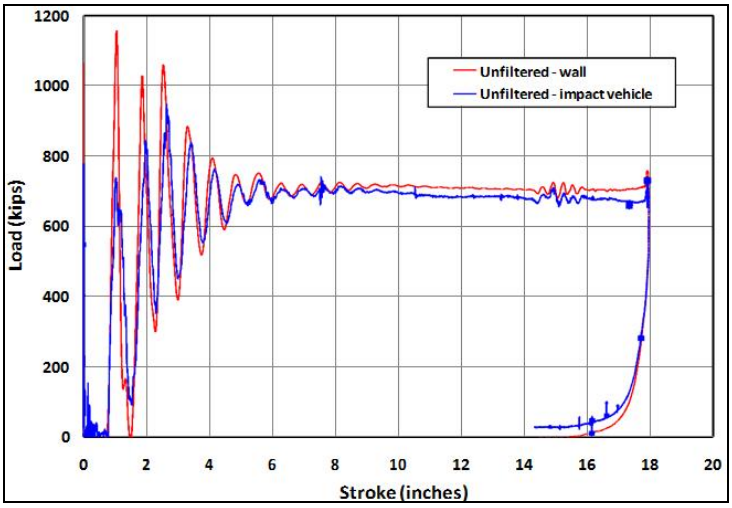

Figure 64. Comparison of Load-Displacement Response Measured at the Instrumented Wall and at the Impacting End of the Vehicle for the First Push-Back Coupler Impact Test

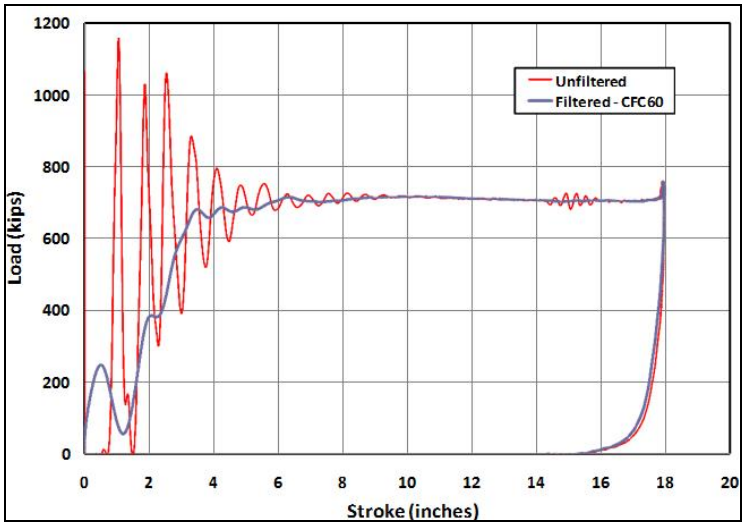

Figure 65. Load-Displacement Response Measured for the First Push-Back Coupler Impact Test (Unfiltered and Filtered at CFC 60)

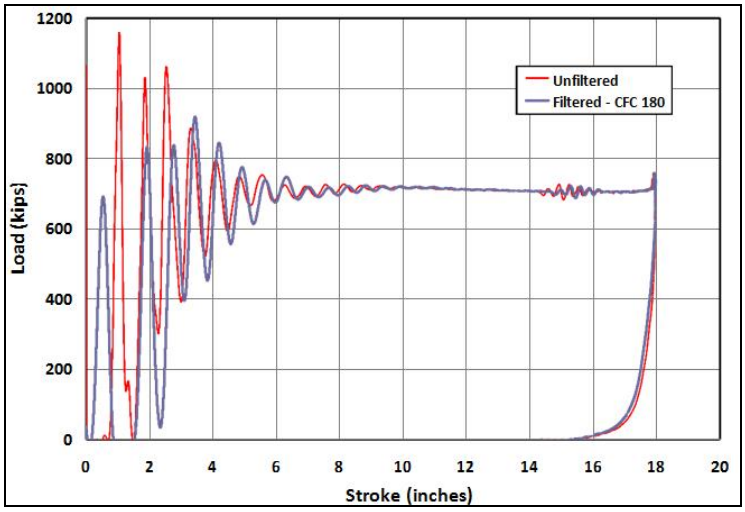

Figure 66. Load-Displacement Response Measured for the First Push-Back Coupler Impact Test (Unfiltered and Filtered at CFC 180)

Key result metrics from the first impact were as follows:

- Total stroke: 454 mm (17.9 inches)
- Push-back trigger force: about 2,970 kN (670 kips)
- Maximum force: 3,300 kN (740 kips)
- Energy absorbed: 1,300 kJ (960 ft-kips).

Note that the trigger force and maximum force listed here are based on data that were filtered at CFC 60.

Figure 67 shows accelerations as a function of stroke; the accelerations are filtered at 40 Hz. These results are consistent with the direct load measurements; e.g., the acceleration corresponding to a load of 700,000 lbf and a vehicle mass of 176,000 lbm is 4.0 g (longitudinal).

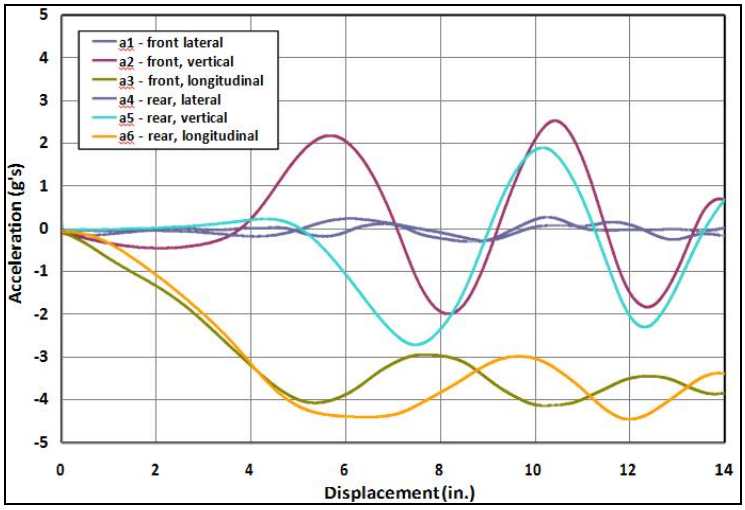

Figure 67. Accelerations vs. Stroke (from the String Potentiometer) for the First Push-Back Coupler Impact Test

Figures 68 and 69 show the test article after the second impact. The sliding lug has been pushed back about 10 inches. The bolts did not all fail completely on a plane parallel to the direction of motion. The three bolts on the left front of the sliding lug all appear to have sheared at roughly a 45 degree angle through half of their thickness (Figure 70). There are also gouge marks on the facing surfaces of the support assembly, as shown in Figure 69, indicating that the sheared bolts scraped along the side of the support assembly as the sliding lug pushed back. In fact, it was not possible to separate the lug from the support assembly immediately after the test because of at least one protruding bolt surface. Figure 71 shows the measured load-displacement plot, in which the load is taken from the load cell set on the wall and the displacement is taken from the string pot at the coupler extension.

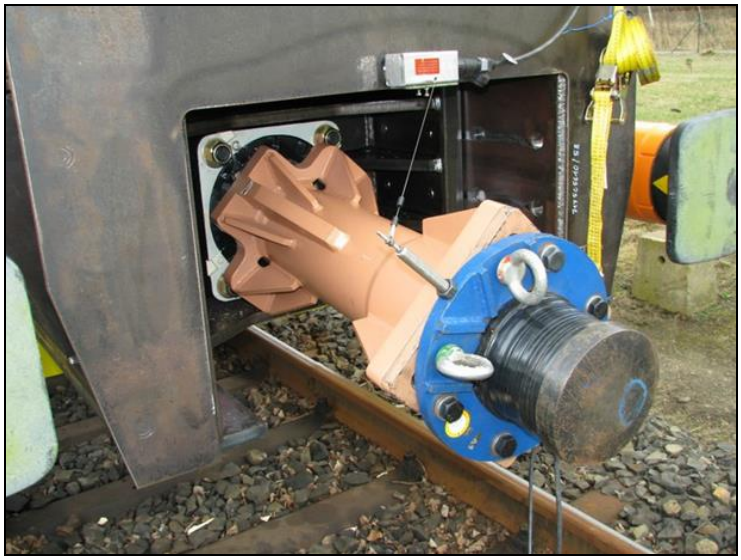

Figure 68. Push-Back Coupler Test Article After the Second Impact

Figure 69. Photograph Showing Gouging Marks in the Coupler Support Assembly After the Second Impact

Figure 70. Photograph Showing All Twelve Failed Shear Bolt Heads
Note that the three shear bolt heads on the bottom right sheared non-uniformly.

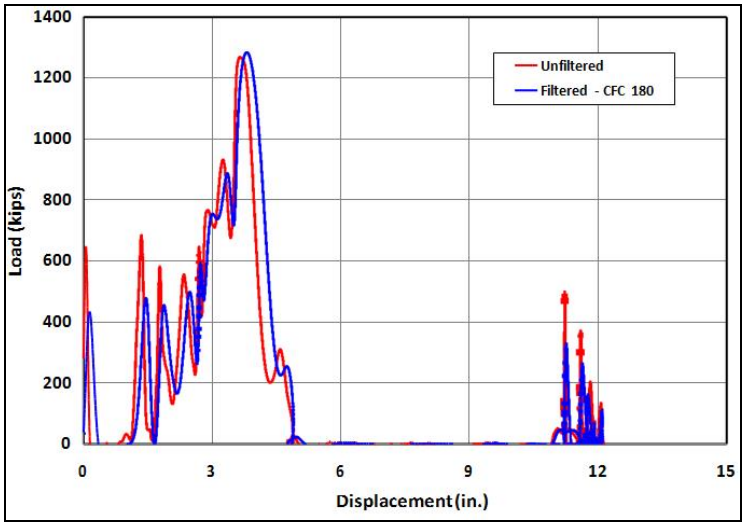

Figure 71. Load-Displacement Response Measured for the Second Push-Back Coupler Impact Test (Unfiltered and Filtered at CFC 180)

Key result metrics from the second impact were as follows:

- Total stroke: 96 mm (3.8 inches), up to complete bolt fracture
- Maximum force: 5,640 kN (1,270 kips)
- Energy absorbed: 165 kJ (120 ft-kips).

Note that the trigger and maximum force listed here are based on data that have been filtered at CFC 180.

5.4.3 Discussion

The push-back coupler test results indicate that the element meets component requirements:

- Push-back trigger load: 2,970 kN (670 kips)
  - Design minimum value: 3,000 kN (600 kips)
  - Design maximum value: 3,560 kN (800 kips)
- Energy absorption: 1,300 kJ (960 ft-kips)
  - Design minimum value, 810 kJ (600 ft-kips).

The exact value of the push-back trigger load is difficult to define because of dynamic effects, but it is certainly within the range of the required load.

Pre-test predictions indicated that the total shear bolt failure load would be about 4,700 kN (1,056 kips). The measured load corresponding to shear bolt failure was 5,640 kN (1,270 kips), which is 20% higher than the expected value. This may be due in part to dynamic effects, but it also could be due in part to the non-uniform shearing of the three forward-left bolts.

The push-back coupler system is designed to permit push-back of the sliding lug by 14 inches, to allow the deformable anti-climber to absorb energy. The lug moved back about 10 inches. It appears from Figure 71 that there was little resistance to push-back motion for the first 5 inches or so, and indications of some resistance at around 5 to 6 inches of push-back, with little resistance thereafter. This resistance may have been due to gouging of the non-uniformly sheared bolts (see Figure 69) or interference between the sliding lug and the support plates. The string pot and ruler measuring sensors showed greater displacement, but some of it was downward motion (in the case of the string pot) and rebound (in the case of the ruler system, which does not record change in direction directly). The measured accelerations indicate that the vehicle pitched down on initial impact but then oscillated up and down without significant pitch after about 8 inches of stroke.

5.5 Deformable Anti-climber Test Description and Results

5.5.1 Test Description

Figure 72 shows a photograph of the deformable anti-climber test article, which is mounted to the load cell sets on the impact wall. The end of the impacting car is flat with no additional structure as shown in Figure 73.

Figure 72. Photograph of the Deformable Anti-Climber Test Article Mounted on the Impact Wall Prior to Impact

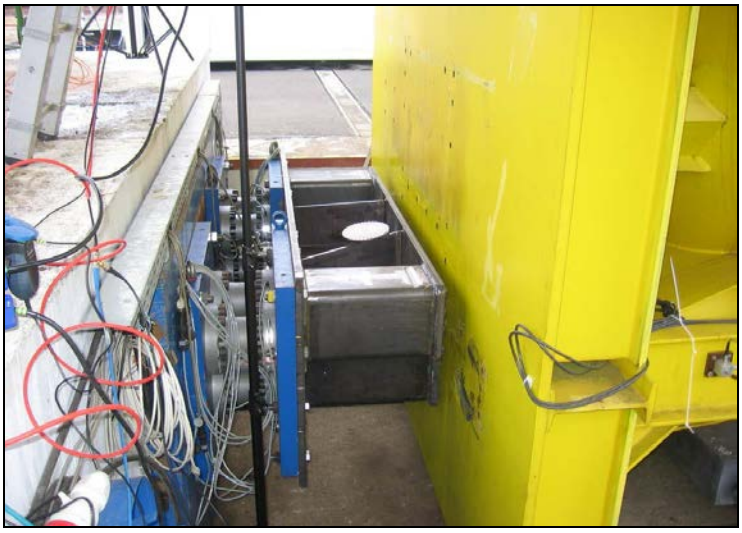

Figure 73. Photograph Showing Both the Deformable Anti-Climber Test Article and the Impact Car Prior to the Test

Energy absorbing buffers were not used in this test, because no additional stroke was available beyond the design crush stroke. The impact speed of the rail car in the single impact was 20.8 km/hr (13.0 mph)—0.8 km/hr greater than the target speed.

5.5.2 Test Observations and Results

Figures 74 and 75 show the test article after the impact. The energy absorption capacity of the test article has essentially been exhausted. The deformation pattern is very symmetric with respect to the centerline. There are small areas of cracking, as is evident in Figure 76, but they are isolated. Figure 77 shows the measured load-displacement plot, in which the load is taken from the load cell set on the wall and the displacement is taken from the ruler on the car. (A

string potentiometer, which was not required but had been added by the test center, did not record data properly.) Figure 78 shows the measured accelerations versus displacement. The mean longitudinal acceleration, about 4 g, is consistent with the acceleration expected from an 800,000 lbf load (800,000 lbf/176,000 lbm = 4.4 g). The front lateral accelerometer recorded a relatively high initial acceleration. This may have been caused by a difference in gap between the end of the test article and the face of the impact car across its width; a gap of about 1 cm was measured prior to the test.

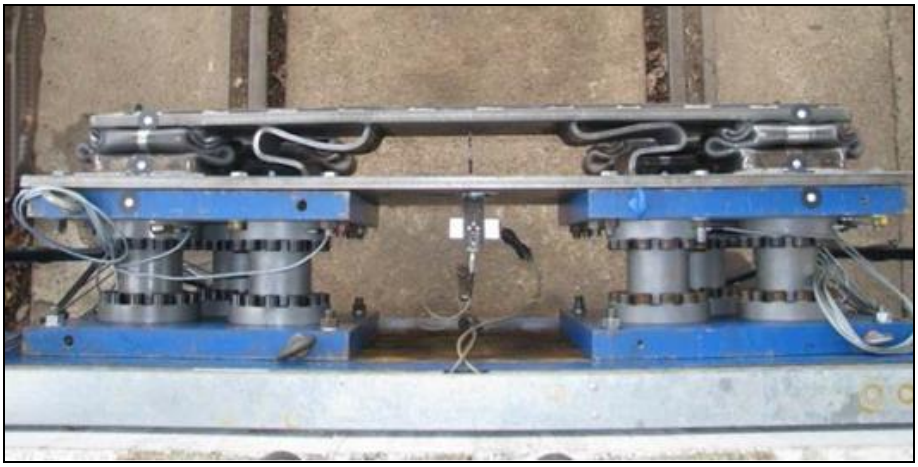

Figure 74. The Deformable Anti-Climber Test Article After Impact (Top View)

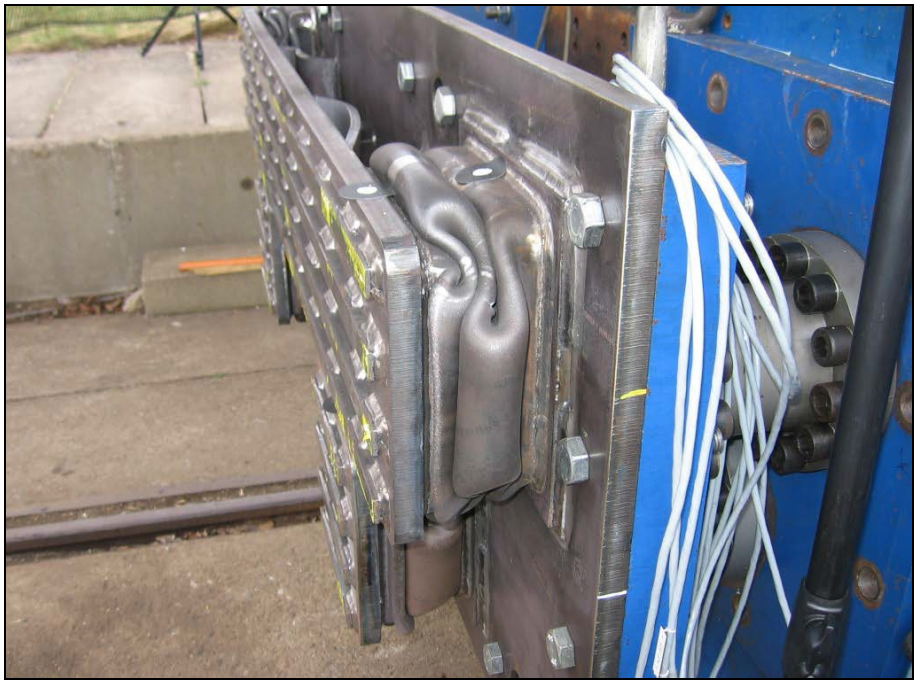

Figure 75. The Deformable Anti-Climber Test Article After Impact (Side View)

Figure 76. Photograph of a Crack in the Deformable Anti-Climber Test Article After Impact

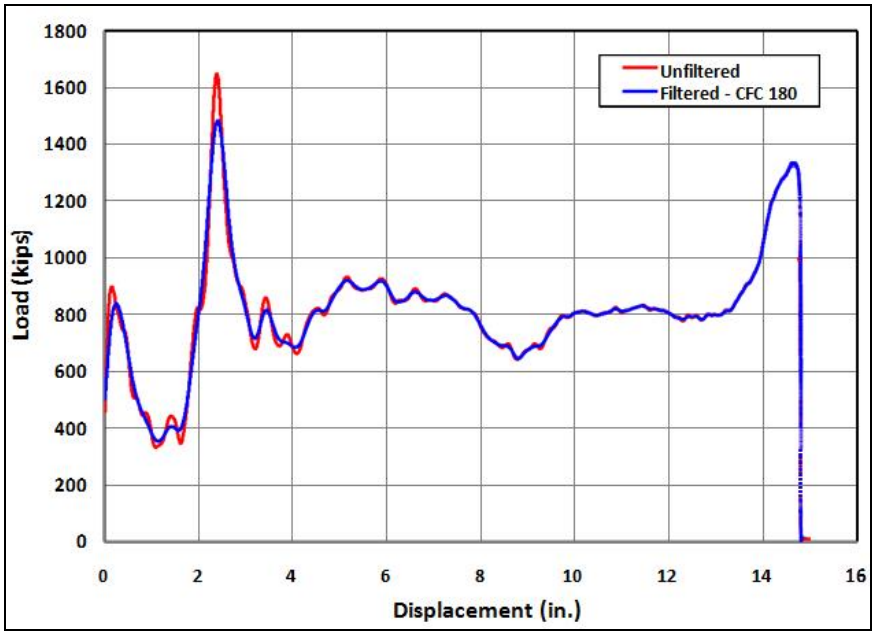

Figure 77. Load-Displacement Response Measured for the Deformable Anti-Climber Test
Unfiltered and filtered at CFC 180. Displacement measured by laser/ruler.

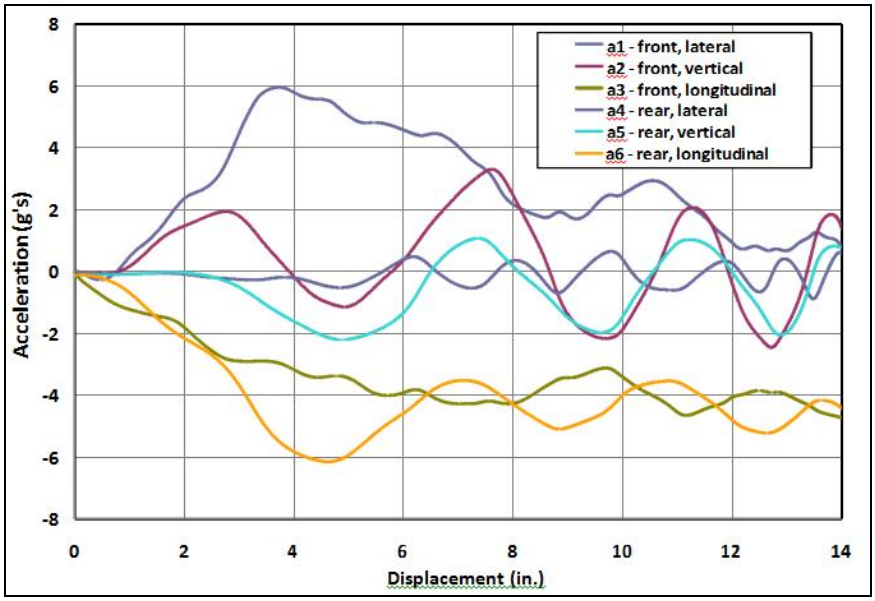

Figure 78. Accelerations vs. Displacement for the Deformable Anti-Climber Impact Test
Displacement measured by laser/ruler.

The key result metrics from the test were as follows:

- Total stroke: 373 mm (14.7 inches)
- Maximum force: 5,960 kN (1,340 kips)
- Energy absorbed: 1,350 kJ (1,000 ft-kips).

Note that the maximum force listed here is based on data that have been filtered at CFC 180. All the welds were inspected after the test and were found to be intact.

5.5.3 Discussion

The deformable anti-climber test shows that the element met the component trigger load requirements and the energy absorption requirement:

- Trigger load: 3,650 kN (820 kips)
  - Design minimum value: 3,560 kN (800 kips)
  - Design maximum value: 5,340 kN (1,200 kips)
- Energy absorption: 1,350 kJ (1,000 ft-kips)
- Design minimum value, 945 kJ (700 ft-kips).

The exact value of the trigger load is difficult to define because of dynamic effects. The deformation is very symmetrical, and the individual tubes show the classic accordion pattern.

6. Comparison of Test Results with Pre-test Predictions

6.1 Push-back Coupler

Due to the low impact speed for the first push-back coupler test, the push-back coupler system was effectively tested in two stages: one stage to exhaust the push-back coupler, and one stage to shear the bolts. Consequently, and in order to compare with model predictions for a single test, the force-displacement results for the two impacts were combined into a single integrated curve. Figure 79 shows such a comparison. In the figure, the test results for the first impact are plotted as measured (see Figure 65). The results for the 2nd impact have been shifted by the extent of permanent deformation predicted in the 1st test—about 15 inches (~18 inches of deformation tube stroke minus ~3 inches of rubber spring elastic recoil) (see Figure 5).

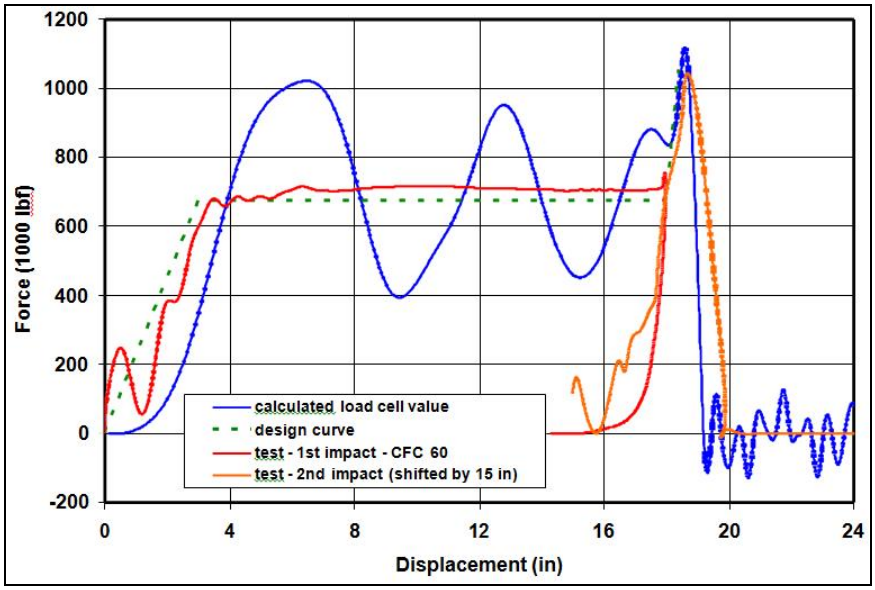

Figure 79. Comparison of Predicted Force-Displacement Behavior with Model Predictions

As noted earlier, model predictions of the force required to break the bolts are based primarily on the assumed shear strength of the bolts: 12 x 88 kips = 1,056 kips. The raw measured peak load associated with bolt failure is approximately 1,260 kips (see Figure 71), nearly 20% higher than the combined assumed shear strength of the bolts. (When filtered at CFC 180, the peak is about the same as it is when unfiltered.) The 20% increase may be due in part to the dynamics of the bolt failure process; however, it is likely that much of the increase is due to the "unclean" nature of the shearing-off process for the left, forward set of three shear bolts (see Figure 70).

In retrospect, a better match between the test result and the design shear strength might have been achieved if additional care had been taken to ensure that the gap between the sliding lug and the side plate of the support assembly—across the shear plane of the shear bolt—was balanced across all the shear bolts. There was some indication during inspection (see Figure 31) that the gap was much smaller on the forward left side of the sliding lug (right side in Figure 31, in which the assembly is shown upside down) than it was on the right side.

This may have been due to the manner in which the shear bolts were tightened. There was a tightening torque specified for each bolt, but there was not a specified tightening order that might have balanced the torque- down of the bolts. Nor were there any procedures—the use of shims, etc.—that might have prevented excessive closing of the gap. The tolerance for the gap is 0.015 +0.075/-0.015. Thus, a completely closed gap is not an indication that the position of the lug with respect to the side plates was out of tolerance. Note also that the shear bolts were designed so that the outer edge of the groove at which the bolt is meant to shear lines up perfectly with the inner wall of the side plate. It is very unlikely that the imbalance caused the groove to be in the wrong position. The non-ideal shearing of these three bolts is more likely due to compressive stresses between the two surfaces that arose when the bolts were tightened, which in turn produced tensile stresses in the bolts that contributed to the observed fracture pattern.

In terms of the mode of deformation, the FEA model did not include pitching motion of the rail car; therefore, the coupler was predicted to move essentially in a longitudinal direction. Test videos indicate that the coupler shank moved longitudinally until near the end of the test, at which point there was a sharp upward motion that caused the feature built into the coupler shank to scrape the underside of one of the sliding sill gussets. One must keep in mind that the forward speed of the coupler with respect to the sliding lug was very small at this point. It is likely that, if the initial impact speed had been sufficiently high, the coupler shank would have impacted the sliding sill mounting block with little such upward movement.

6.2 Deformable Anti-Climber

In Figure 80, the measured force-displacement curve for the deformable anti-climber test is compared with the pre-test prediction curve. The predicted displacement for the measured impact speed of 20.8 km/hr was 14.4 inches, as indicated in the figure. The measured maximum displacement was approximately 14.9 inches.

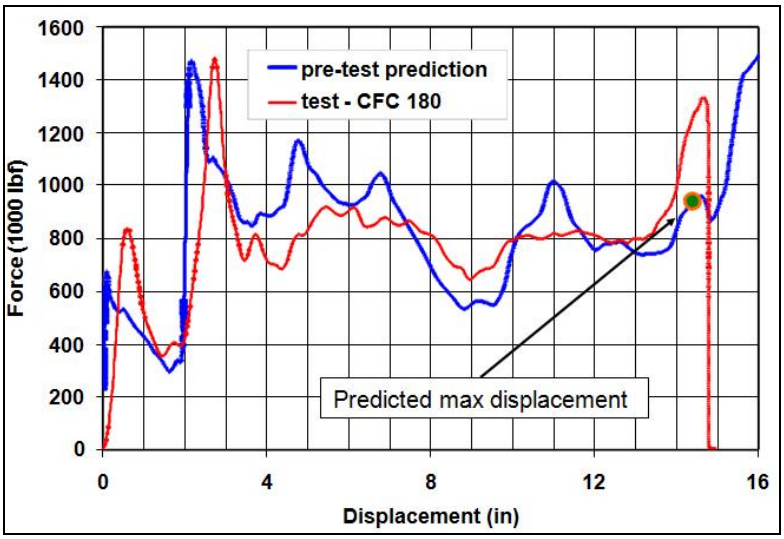

Figure 80. Comparison of Measured Force-Displacement Curve for the Deformable Anti-Climber Test With the Pre-test Prediction

The predicted displacement for the measured impact speed of 20.8 km/hr is indicated.

The difference between the measured and predicted displacement can be attributed to two factors:

- Over the first 4 inches of displacement, the predicted average load is approximately 740 kips, and the average measured load is approximately 680 kips. The shape of the test curve indicates that there is more compliance in the system than the FEA model predicts, as one might expect, due to non-uniformities in the initial geometry of the structure, misalignment with the test vehicle, etc. The build-up of load associated with impact of the two respective sets of crush tubes appears to be more gradual than the model predicts. This leads to an offset of about 0.5 inches or so in the displacements at which the peaks occur, and the additional compliance lowers the average load.
- Over the displacement range of 4–12 inches, the predicted average load is approximately 840 kips, but the measured average load is only 800 kips. After the impact of the second set of tubes, all four tubes fold in a manner that is consistent with both model predictions and the results of quasi-static compression tests. The 40-kip difference between the predicted and average loads can be attributed to differences between the modeled and actual hardening and failure behavior of the A572-50 material, as well as imperfections in the initial geometry of the tubes. Buckling processes can be quite sensitive to geometrical imperfections, which could tend to lower the load required to fold the tube.

When the two factors are summed, it can be seen that, after 12 inches of crush, an additional 560 in-kips of kinetic energy must be absorbed in the test. This extra energy is consistent with the extra 0.5 inches of crush occurring at an average force of 1,000 to 1,100 kips.

In terms of deformation, it is most useful to compare the model predictions with test results *for equivalent extents of displacement*. Therefore, while the model predicted a final displacement of only 14.4 inches for the measured impact speed of 20.8 km/hr, model predictions were compared with test results at a total displacement of 14.7 inches. The comparisons are shown in Figures 81, 82, and 83.

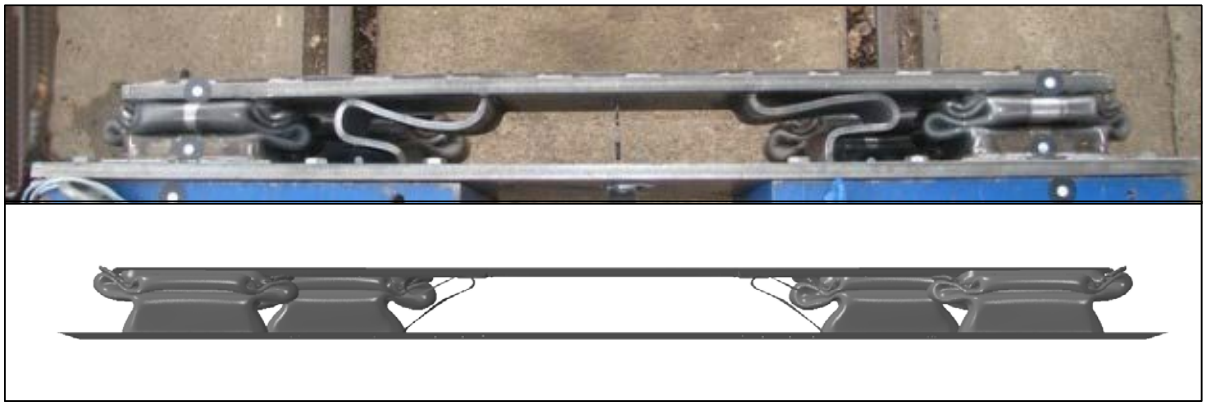

Figure 81. Comparisons of Model Prediction of Test Article Deformation at 14.9 Inches With Post-test Results: View From Above Test Article

The overhead view shown in Figure 81 indicates that the model captures the essential features of the deformation quite well. The predicted folding pattern of the tubes is identical to the actual pattern, although in the model the “ears” that are formed on the sides of the tubes tend to be oriented more toward the impacted end of the tube than they actually are in the test. The most

significant difference between the predicted and actual modes of deformation is that the angled support plates fold in a different manner. The model predicts that the front of the plate will fold outward and the back of the plate inward. The test result is the opposite. This difference is not surprising, and it is likely due to geometrical imperfections and/or pre-stresses in the plates that result from welding. More importantly, it is unlikely that the direction of folding has a significant effect on the transmitted load.

The isometric view shown in Figure 82 presents an alternate view of the folded tube. Here again one can see the difference in the orientation of the side folds. Overall, however, the model seems to capture the deformation mode quite well. The folding pattern observed dynamically is also quite similar to the folding pattern from the quasi-static crush test (see Figure 21).

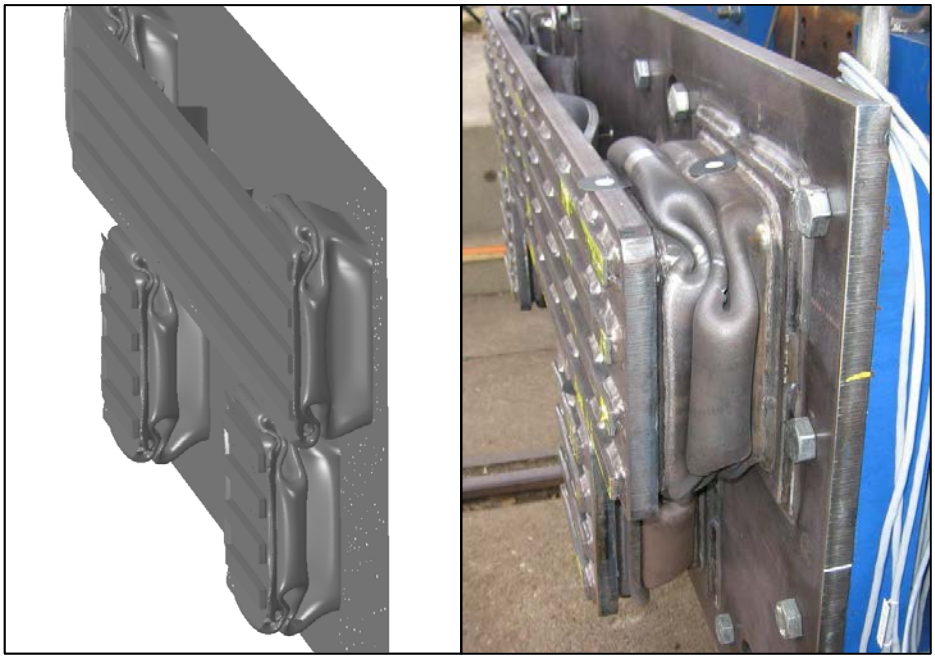

Figure 82. Comparison of Model Prediction of Test Article Deformation at 14.9 Inches With Post-test Results: Isometric View Focusing on Left Upper Crush Tube

As expected, there were several locations of localized fracture. Without exception, they occurred in the corners of the crush tubes, where severe plastic strain arises as the tube folds. Not only were such fracture locations predicted (see Figure 83), they were also observed in identical locations during the quasi-static tests. Given the extremely large plastic strain and complex deformation patterns—and therefore large stress triaxiality—that arise as the tubes crush, such localized fractures will occur despite the high inherent ductility of the A572-50 material. Moreover, these fractures do not appear to cause eccentric crush of the tubes, nor do they appear to hinder the absorption of energy that occurs as the tubes fold.

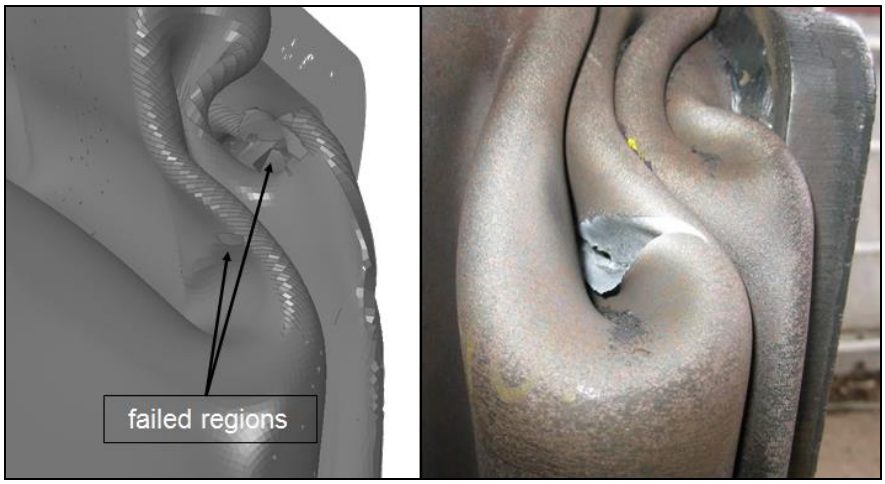

Figure 83. Comparisons of Model Prediction of Test Article Deformation at 14.9 Inches With Post-test Results: Upper Right Tube Showing Localized Fracture Inside a Fold

7. Summary and Conclusions

As noted in the introduction, the purpose of the testing program conducted under this Option A portion of the overall program was to verify certain performance characteristics of the two crashworthy components relative to requirements.

While there were some issues that were revealed through testing, overall the tests were successful in demonstrating the effectiveness of the two concepts. Test results were in very good agreement with model predictions both in terms of force-displacement behavior and modes of deformation. It would have been preferable to have tested the push-back coupler in a single test, but the results of the two impacts were sufficient as they produced the desired measurements when combined.

A few lessons learned during the program worth noting:

- The materials testing and subcomponent testing were well worth the time and investment that were required. The tensile tests were relatively easy to do, and produced data that were invaluable to the FEA modeling component of the program. Likewise, the subcomponent tests were completed relatively quickly and at relatively low cost, and revealed a design flaw that likely would have rendered the much more costly deformable anti-climber dynamic impact test unsuccessful. The FEA modeling that was undertaken as part of the subcomponent test program also helped to guide the more complex FEA of the deformable anti-climber test article, which provided much confidence in the outcome going into the tests.
- The subcomponent tests also aided in our decision to use four slots for the crush tube design rather than two slots, so as to minimize the peak in load associated with the impact of the second set of tubes.
- The push-back coupler test revealed a weakness in the assembly process for the shear bolt-fuse system. In retrospect, it would have been better to have included a control on the order in which the bolts were tightened and/or a control on the sliding sill-to-side plate gap so as to prevent closing of the gap during installation. Given the weight of the sliding lug assembly, it would have been prudent to re-inspect the shear bolt system after the assembly was turned right-side up following bolt installation.
- The test facility's prior experience was relied upon for determining the impact speed. Particularly in light of the change that was made to the suspension system of the impact vehicle, one or two speed test runs prior to the actual test should have been performed.

Abbreviations and Acronyms

AC	alternating-current
AT	Auto-Tension (system)
CFC	Channel Frequency Class
DC	direct current
DP	distributed power
EPA	U.S. Environmental Protection Agency
FEA	Finite Element Analysis
FRA	Federal Railroad Administration
Hz	Hertz
kV	kilovolt
mph	miles per hour
MVA	megavolt-amperes
MW	megawatts
NEC	Northeast Corridor
OCS	overhead contact system
PPP	public private partnership
PTC	Positive Train Control
SLAs	service level agreements
USDOT	U.S. Department of Transportation
VSL	value of a statistical life

References

1. APTA PRESS Task Force and APTA Commuter Rail Executive Committee. (2006). *Standard for the design and construction of passenger railroad rolling stock*," 11. APTA PR-CS-S-034-99, Rev 2. Washington, DC: The American Public Transportation Association, http://www.apta.com/resources/standards/Documents/APTA-PR-CS-S-034-99.pdf.

2. Association of American Railroads. (December 2004, revised 2008). AAR S-580 Standard, "Locomotive Crashworthiness Requirements."

3. TIAX Final Report to Volpe Center. (2009). Development and fabrication of state-of-the-art end structures for Budd M1 cars. Contract DTRS57-04-D-30008 (TO #7).

4. Llana, P., & Stringfellow, R. (2014). Development, fabrication, and testing of locomotive crashworthy components. DOT/FRA/ORD-14/38, http://ntl.bts.gov/lib/54000/54400/54413/Locomotive_Crashworthiness_20141110_final.pdf.

5. Tyrell, D., Severson, K., Marquis, B., Martinez, E., Mayville, R., Rancatore, R., Stringfellow, R., Hammond, R., & Perlman, A.B. (1999). "Locomotive crashworthiness design modifications study," *Proceedings of the 1999 IEEE/ASME Joint Railroad Conference, Institute of Electrical and Electronics Engineers*, Catalog Number 99CH36340, http://ntl.bts.gov/lib/22000/22600/22657/locsumry.pdf.

6. National Transportation Safety Board. (2012). *Collision of BNSF coal train with the rear end of standing BNSF maintenance-of-way equipment train, Red Oak, Iowa, April 17, 2011*. NTSB Railroad Accident Report, NTSB/RAR-12/02, PB2012-916302. Washington, DC.

7. Mayville, R., Stringfellow, R., Johnson, K., & Landrum, S. (2003). *Crashworthiness design modifications for locomotive and cab car anticlimbing systems*. Washington, DC: Federal Railroad Administration. DOT/FRA/ORD-03/05, http://ntl.bts.gov/lib/34000/34400/34402/DOT-VNTSC-FRA-03-01.pdf.

8. American Public Transportation Association. (2012). "Recommended practice for push-back couplers in passenger rail equipment." APTA PR-RP-C&S-019-11, http://www.apta.com/resources/standards/Documents/APTA%20PR-CS-RP-019-12.pdf.

9. APTA PRESS Task Force and APTA Commuter Rail Executive Committee. (2006). *op. cit.*

10. American Public Transportation Association (2012), *op. cit.*

11. TIAX Final Report to Volpe Center (2009), *op. cit.*

12. Code of Federal Regulations, Title 49, Part 229, "Railroad Locomotive Safety Standards."

13. APTA PRESS Task Force and APTA Commuter Rail Executive Committee. (2006). *op. cit.*

14. American Public Transportation Association. (2012). *op. cit.*

15. Lllana and Stringfellow. (2014). *op. cit.*

16. TIAX Final Report to Volpe Center. (2009). *op. cit.*

17. Lllana and Stringfellow. (2014). *op. cit.*

18. Federal Railroad Administration (2013). "Prototype locomotive crashworthy component drawings." http://www.fra.dot.gov/eLib/Details/L04646.

19. Lllana and Stringfellow. (2014). *op. cit.*

20. Lllana and Stringfellow. (2014). *op. cit.*